ISSN 0332-5

Norwegian Geophysical Society

Geophysica Norvegica

I. KANESTRØM, K. PEDERSEN & H. SKÅTUN
Major stationary ridges and troughs at 500 mb
1

K. STAMNES
A unified theory of interhemispheric electron transport and energy degradation
41

VOL. 33 NO. 1. 1985
UNIVERSITETSFORLAGET

GEOPHYSICA NORVEGICA. VOL. 33. NO. 1. PAGES 1–51 1985 UNIVERSITETSFORLAGET

Geophysica Norvegica

is a journal of geophysics, issued under the auspices of the Norwegian Geophysical Society. *Geophysica Norvegica* is mainly intended as a journal for Norwegian authors, but papers from other authors may be accepted provided that the work has been carried out at a Norwegian institution or its content has a special relevance to Norway.

PUBLISHER

Universitetsforlaget: P.O. Box 2959, Tøyen, 0608 Oslo 6, Norway
P. O. Box 258, Irvington-on-Hudson, New York 10533

SUBSCRIPTION

Geophysica Norvegica is published at irregular intervals. Order from the Publisher, Universitetsforlaget.

CONTRIBUTIONS

Manuscripts conforming with the rules on page 3 of the cover should be addressed to the editor. The editorial board will appoint referees, who will ensure that the paper meets a sufficiently high scientific standard.

GEOPHYSICA NO 1—A

Major stationary ridges and troughs at 500 mb

INGOLF KANESTRØM, KAARE PEDERSEN & HELGE SKÅTUN
Institute of Geophysics, University of Oslo

Kanestrøm, I, Pedersen K. & Skåtun, H. Major stationary ridges and troughs at 500 mb. *Geophysica Norvegica*, Vol. 33, No. 1, pp. 1–40, 1985.

Daily 500 mb geopotential heights at 12Z for the period January 1, 1946, through May 31, 1980 are analysed. A Fourier expansion is made along the latitude circles, retaining only the first four wavenumbers. From the height field made up of these four waves, the large scale quasi-stationary ridges and troughs in middle latitudes are determined. The distributions of these ridges and troughs with respect to position, time of the year and duration are discussed.

The troughs may be grouped in two preferred sectors, the Atlantic and the Pacific regions. The ridges are found in three different sectors, the Pacific, the Atlantic–European and the Asian regions. While 82% of the troughs are located in the Pacific region, most of the ridges (67%) are located in the Atlantic–European region. The events are most frequent in winter-time, November through March, for the Atlantic and Pacific regions. In the Asian region, however, there is a maximum occurrence of ridges in April–May and November. The duration probability for the events may be estimated from first order Markov chain.

A wave description indicates that the events are associated with an amplification of the wave amplitudes near the normal position. In addition the analysis shows that relatively small phase shifts may intensify the ridge or trough. The wave number four is of relative great importance in summer season and also for the ridge events in the Asian region in the spring and fall seasons.

I. Kanestrøm, Institute of Geophysics, University of Oslo, P.O. Box 1022, *Blindern*, 0315 *Oslo* 3, *Norway*

1. INTRODUCTION

The phenomenon termed blocking has been studied since it was first noted by Garriot (1904), and since then there have been various subjective and objective definitions of blocking. However, the main definition from the synoptic point of view has been a quasi-stationary high pressure cell persisting in a region where westerly winds are normally found. More precise definitions are given by Rex (1950), Namias (1964), Austin (1980) and Lejenäs & Økland (1983).

The flow pattern with a quasi-stationary high pressure cell can be described in three ways, the 'synoptic' description, the 'wave' description and the 'local index' description. The first two have been discussed by Austin (1980). The 'local index' definition is based upon the splitting of the jet stream, and in the blocked area the mean zonal velocity (index) vanishes, or the zonal wind is easterly. This description has been discussed by Lejenäs & Økland (1983).

In later theoretical studies by Dole (1978, 1983), Charney et al. (1981) and Frederiksen (1982), the blocking phenomenon has been associated with persistent large height anomalies in the 500 mb flow. By this definition, also situations with strong zonal flows may be defined as blocking if the positive anomalies happen to be in the positions where the large troughs are normally found.

In this paper we have studied large-scale persistent quasi-stationary ridges and troughs in the Northern Hemispheric 500 mb flow. The term 'blocking' is normally associated with the ridges, but also the troughs have the effect of blocking the westerly flow in the middle latitudes.

These large-scale ridges and troughs will be referred to as Major Stationary Ridge (MSR)-events and Major Stationary Trough (MST)-events, respectively. The term 'event' will generally refer to any of these cases. In section 3 our definition of MSR- and MST-events is given and compared with definitions of blocking given by other authors.

In section 4 we will study the occurrence of these events. The distribution with respect to position, time of the year and duration will be discussed. In section 5 the anomaly patterns associated with these events are considered, and in section 6 a wave description is given.

2. THE DATA

The data set used in this study has been supplied by NCAR, and contains daily 500 mb geopotential heights at 00Z and 12Z on grid form. The grid used is the NMC 47 × 51 pts. octagonal grid (Jenne 1975), and the data set covers the period from January 1, 1946 through May 31, 1980. We have used only the 12Z (15Z for one period) observations, because the heights at 00Z were missing during some periods. Only 179 days (out of 12,570) were missing at 12Z.

The data were first interpolated from the NMC-grid to a 5° × 5° latitude-longitude grid from 25° N to 90° N, using a 16-point Bessel interpolation scheme. From these data a Fourier expansion was made along the latitude circles, retaining only the first 4 wavenumbers. The coefficients were found using the simple formulas

$$a_n(\varphi_j) = \frac{1}{36}\sum_{i=1}^{72} z(\lambda_i, \varphi_j) \times \cos(n\lambda_i) \qquad n = 0, 1, 2, 3, 4 \tag{1}$$

$$b_n(\varphi_j) = \frac{1}{36}\sum_{i=1}^{72} z(\lambda_i, \varphi_j) \times \sin(n\lambda_i) \qquad n = 1, 2, 3, 4.$$

In this manner the height field becomes zonally smoothed, and the smoothed height value at some longitude λ_i and latitude φ_j is given by:

$$z^*(\lambda_i, \varphi_j) = \frac{a_0(\varphi_j)}{2} + \sum_{n=1}^{4} a_n(\varphi_j) \times \cos n\lambda_i + b_n(\varphi_j) \sin n\lambda_i \tag{2}$$

where

$$\varphi_j = [20 + 5j]°\text{N} \qquad j = 1, 14$$

$$\lambda_i = [5 \cdot (i - 1)]\,°\text{E} \qquad i = 1, 72.$$

This study is part of a project which attempts to give an objective numerical description of different types of large scale flow patterns in the northern hemisphere. In order to use as few parameters as possible in this description, we have chosen to retain only four wavenumbers at each latitude. Also the synoptic and theoretical studies of the major stationary ridges and troughs indicate that at least in the winter season stationary waves of wavenumber 5 and larger do not occur north of 45° N. This has been shown theoretically by e.g. Hoskins & Karoly (1981) for a barotropic atmosphere.

From the z*-field we have found the daily minima and maxima along latitude circles. This has been done for the latitudes 40° N, 50° N and 60° N. The positions and deviations from the zonal average for these extrema have been plotted in a time-longitude diagram (Hovmøller diagram) for each of these latitudes. The resolution in longitude is 3 degrees, and 1 m in the heights.

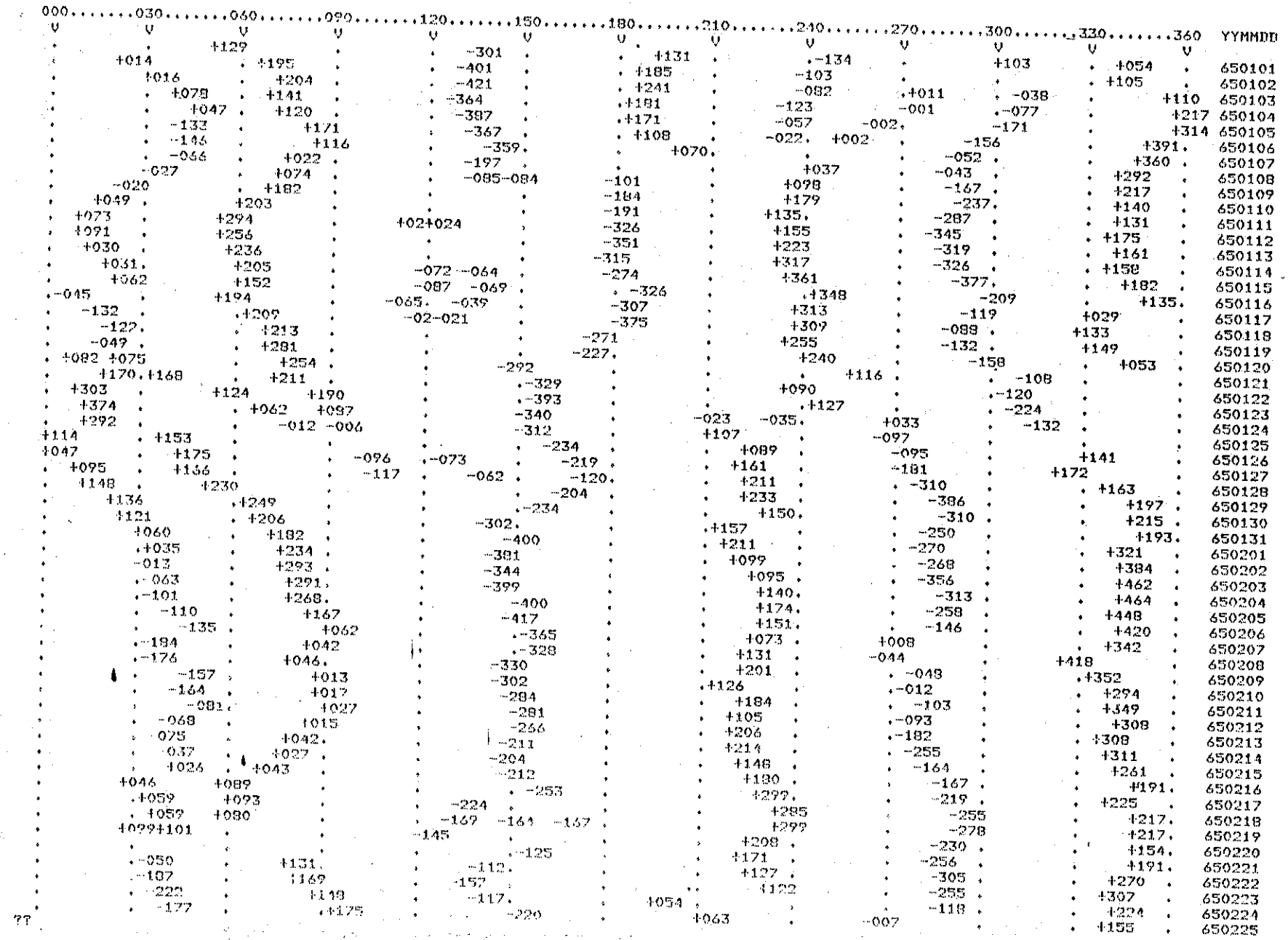

Fig. 1. Hovmøller diagram for the MSR event at 50° N, Feb. 1–15, 1965. The longitude is given at the top of the diagram and the date on the right. The numbers give the maximum (minimum) value of the amplitude relative to the zonal mean field, and the position of the sign indicates the longitude.

From this diagram (see Fig. 1) the stationary ridges and troughs are easily found.

3. DEFINITION OF MSR/MST-EVENTS

In this study we will use the synoptic blocking description approach to describe a MSR or MST event. Such an event is defined as a large, positive or negative, geopotential height deviation from the zonal mean at the latitudes 40° N, 50° N and 60° N, where we normally find the westerlies. The deviation must fulfil certain criteria on amplitude, persistence and stationarity to be defined as an event.

Our criteria are that a major ridge or major trough with an amplitude of two standard deviations or greater shall persist for 10 days or more. The amplitude must also exceed 3 standard deviations at least one day in this period.

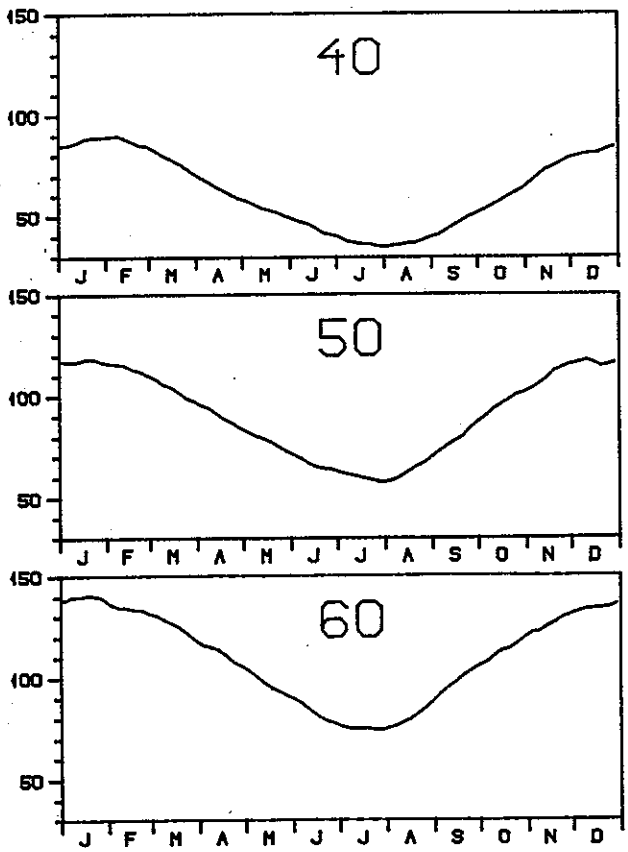

Fig. 2. The standard deviation for the height deviation from the zonal mean field.

The criteria on stationarity are given both as a limit on the total displacement (in the longitudinal direction) of the extremum point during the period and on the displacement from one day to the next. The peak point is not allowed to move more than 36 degrees during the whole period and 18 degrees in one day.

Relating the amplitude threshold to the standard deviation, which varies over the year, will give stronger conditions on amplitude when the amplitudes normally are large (e.g. winter) than when we normally have small amplitudes (summer). A constant threshold value would have preferred winter events and neglected summer events. Figure 2 shows the standard deviations used at 40° N, 50° N and 60° N.

These standard deviations are found in the following manner. Let z^* denote the Fourier expansion of z around a latitude circle and let z_0 denote the zonal mean. The standard deviation σ is then given by

$$\sigma^2(\varphi) = \frac{1}{2\pi}\int_0^{2\pi} \mathrm{Var}(z^*(\lambda, \varphi) - z_0(\varphi))\, d\lambda. \tag{3}$$

By the properties of the Fourier expansion, this can be written

$$\sigma^2(\varphi) = \frac{1}{2}\sum_{k=1}^{4} \mathrm{Var}(a_k) + \mathrm{Var}(b_k). \tag{4}$$

The variances are given by

$$\mathrm{Var}(x) = \widetilde{(x - \bar{x})^2}. \tag{5}$$

The quantity $\bar{x}$ is referred to as the climatological mean of x, and is here defined as the average of x over the years 1946 through 1979 for a particular day of the year. This definition will be used in later chapters. In order to get more observations for each sample we have 5-days means of the variances. In Fig. 2 the standard deviations are computed

from moving averages of the variances over 30 days (6 pentades).

The limit on stationarity of 18 degrees movement during one day might seem rather large. The values 18 and 36 degrees are chosen rather arbitrarily, but we have compared with Charney et al. (1981) and used criteria that are weak enough to include all the episodes with sufficient amplitude found by them (see their tables 2 and 3). We have seen from our case studies that the ridges and troughs having these rapid changes in the position of the extremum are broad features. The ridge or trough is stationary itself, but the values of the deviation from the zonal mean are close to the extreme value also at longitudes somewhat away from the extremum. When one of these values exceeds the former extremum, it shows up as a rapid movement of the peak position.

4. FREQUENCY OF BLOCKING AS A FUNCTION OF SPACE AND TIME

Grouping of the events in longitudinal regions

In this section we examine the frequency of MSR and MST events at 500 mb as a function of space and time. The criteria given in section 3 are used, and the events are identified from the Hovmøller diagrams. The z*-fields averaged over the duration of each event are computed. These fields are denoted $\bar{z}^*(\lambda, \varphi)$.

The amplitude of $\bar{z}^*$ for each event is calculated. This is the maximum deviation from the zonal mean of the $\bar{z}^*$-field. We have also found it convenient to have a climatological reference level, so we have computed the

Table 1a

Ridges in the Atlantic-European region (30° W–30° E), winter season in the years 1946–1980.

Period	Days	$\delta\lambda,\Delta\lambda$	Position of ridges	Amplitude	Position of anomaly	Extreme value
460114–460128	15	9,33	15E,60	379	20E,60	257
460209–460222	14	9,15	15W,50	369	20W,55	234
461206–461215	10	15,30	30E,70	381	40E,70	325
461229–470112	15	9,27	35E,65	340	35E,65	280
470118–470127	10	9,12	5W,65	385	10W,65	286
471210–471225	16	9,21	15W,55	371	20W,60	239
480214–480229	16	6,15	5W,60	365	5W,60	221
481201–481211	11	6,12	15E,55	306	20E,55	208
481217–481228	12	15,21	5E,60	377	5E,60	248
490108–490118	11	6,21	20W,50	394	30W,50	270
490120–490207	19	12,27	0 ,55	347	0 ,55	198
490213–490223	11	9,30	5E,50	361	10E,50	243
500118–500128	11	9,24	10E,60	416	15E,65	295
511212–511224	13	6,24	0 ,50	281	15E,55	133
520218–520301	13	9,18	15W,55	349	20W,55	212
521201–521210	10	6,27	15W,60	336	25W,65	263
530117–530208	23	6,27	15W,50	303	20W,55	175
530212–530228	17	6,27	5W,55	322	5W,55	175
531205–531217	13	9,36	20E,65	402	20E,65	310
531218–540111	25	15,33	10W,55	318	15W,55	171
541217–541227	10	6,9	20W,50	391	30W,50	256
560202–560211	10	12,30	10W,60	343	5W,60	210

Table 1c

Ridges in the Atlantic-European region, summer season in the years 1946–1979.

Period	Days	$\delta\lambda,\Delta\lambda$	Position of ridges	Amplitude	Position of anomaly	Extreme value
470621–470702	13	12,21	25E,60	188	20E,60	148
470820–470830	11	12,18	15E,65	236	5E,65	192
530617–530630	14	9,33	20E,70	259	15E,70	238
550809–550828	20	9,21	20E,60	228	15E,60	180
560606–560616	11	15,30	35E,60	239	35E,65	178
590812–590822	11	9,24	25E,65	210	25E,65	155
630528–630608	12	12,27	5E,65	256	5E,65	212
710706–710715	10	18,21	5W,50	184	10W,55	180
760624–760703	10	6,15	5E,55	207	5E,55	168

Table 1d

Ridges in the Atlantic-European region, autumn season in the years 1946–1979.

Period	Days	$\delta\lambda,\Delta\lambda$	Position of ridges	Amplitude	Position of anomaly	Extreme value
461007–461022	16	15,36	10W,65	336	15W,65	259
481123–481203	11	9,30	5E,60	349	5E,60	240
491008–491017	10	9,27	10E,60	244	10E,55	104
510929–511017	19	9,27	15E,60	352	20E,60	231
521103–521113	11	9,15	25W,55	298	25W,55	227
530928–531014	17	9,36	5E,55	250	5E,55	129
531011–531107	28	15,27	25E,60	323	35E,65	208
531104–531122	19	6,18	5E,50	285	5E,50	183
551116–551209	24	12,27	10W,55	314	10W,55	172
561122–561209	18	9,27	15W,50	310	20W,50	149
571110–571206	27	12,27	0 ,60	327	0 ,60	217
580828–580907	11	9,36	15E,65	246	10E,65	203
580910–580920	11	9,30	5E,60	200	5E,65	149
581015–581029	15	6,21	5W,55	269	10W,55	144
581116–581204	19	9,33	0 ,60	348	5E,60	231
590929–591009	11	6,12	5E,65	310	5E,65	220
610928–611011	14	6,15	25E,65	310	30E,65	234
620925–621009	15	9,27	25E,60	308	30E,60	221
621010–621027	18	6,30	5W,55	290	10W,55	167
621124–621206	13	12,27	0 ,55	358	5E,55	226
630912–630923	12	12,24	10E,55	230	10E,55	160
631019–631030	12	15,36	15E,60	282	15E,60	143
641027–641110	15	12,36	0 ,60	337	5W,60	226
641117–641126	10	6,15	10W,50	325	10W,50	180
651016–651026	11	6,15	5E,60	327	5E,60	194
660913–660927	15	6,18	10W,55	205	20W,55	162
661023–661102	11	12,30	20W,60	282	30W,60	241
671114–671208	25	15,33	15W,50	311	20W,55	168

Table 1d—*continued*

Period	Days	$\delta\lambda,\Delta\lambda$	Position of ridges	Amplitude	Position of anomaly	Extreme value
681113–681127	15	12,33	20E,60	304	20E,60	205
690922–691004	13	12,24	5W,50	167	10W,50	96
691013–691022	10	12,18	15E,55	277	15E,55	147
691023–691103	12	9,15	10W,50	330	10W,50	215
701008–701017	10	12,36	10E,60	254	5E,60	118
721014–721023	10	6,12	20W,55	339	25W,55	286
721031–721109	10	6,6	5W,50	300	0 ,50	201
731107–731208	32	12,21	15W,50	289	15W,50	147
741017–741029	13	6,15	25W,50	262	30W,50	200
751019–751104	17	9,27	10E,60	291	15E,60	153
761115–761124	10	6,21	10W,55	325	10W,55	188
771015–771027	13	6,9	10E,60	261	10E,60	126
781015–781103	20	12,36	10W,50	241	15W,50	133
781104–781118	15	9,21	10E,55	285	15E,50	189

the maximum value of this amplitude is given in column four. In the last two columns we give the maximum or minimum values of the anomaly associated with the MSR or MST events, respectively, and the positions of these local extrema.

The events are distributed in groups according to the sector in which they occur (see Tables 9 and 10). Most of the major stationary troughs are located in two sectors around 160° E and 65° W, respectively. In the tables these sectors are named as Pacific and Atlantic region. For the ridges, the classification is more complex. However, we have found that a distribution of the ridges into three sectors is sufficient, namely the Atlantic-European region (30° W–30° E), the Asian region (35° E–80° E) and the Pacific region (100° W–170° W). Two ridges at 125 and 130° E are included in the Asian group. Charney et al. (1981) state that some of the blocking events for the winter seasons they studied may be explained as an amplification of the normal patterns. We will here

Table 2a

Ridges in the Asian region (35° E–80° E), winter season in the years 1946–1980.

Period	Days	$\delta\lambda,\Delta\lambda$	Position of ridges	Amplitude	Position of anomaly	Extreme value
460220–460305	14	18,36	65E,55	215	70E,60	139
501213–501224	12	12,12	55E,55	371	55E,60	265
550112–550122	11	12,18	80E,55	314	85E,60	237
590106–590115	10	6,6	70E,55	350	70E,55	268
601226–610112	18	12,18	55E,55	264	55E,55	176
651124–651208	15	6,15	65E,50	259	65E,50	149
691125–691208	14	9,12	65E,55	394	65E,60	301

Table 2b

Ridges in the Asian region, spring season in the years 1946–1980.

Period	Days	$\delta\lambda,\Delta\lambda$	Position of ridges	Amplitude	Position of anomaly	Extreme value
510325–510408	15	6,12	55E,55	342	55E,55	242
520518–520602	14	6,30	70E,55	278	70E,60	221
530513–530522	10	9,36	40E,55	286	40E,55	171
540223–540311	17	9,36	50E,60	271	55E,60	198
540501–540511	11	12,24	35E,60	256	35E,65	151
570411–570422	12	15,33	55E,55	201	45E,70	150
570505–570515	11	9,30	50E,60	272	60E,65	196
580520–580602	13	9,21	40E,55	208	40E,50	124
600406–600417	12	9,30	50E,60	271	45E,60	175
610519–610529	11	9,18	75E,50	180	80E,50	87
620314–620325	12	6,15	75E,55	269	90E,65	215
630504–630517	14	18,24	35E,60	229	35E,65	125
660327–660408	13	9,27	55E,60	304	55E,60	222
680402–680411	10	12,30	60E,55	237	60E,55	118
680501–680512	12	9,12	55E,55	246	60E,55	130
690423–690503	11	18,33	50E,50	167	40E,50	75
700304–700315	12	9,15	55E,60	308	55E,60	248
700331–700413	14	12,18	65E,55	222	70E,55	109
720419–720502	14	6,15	75E,50	255	80E,50	149
730406–730419	14	6,15	65E,55	280	65E,55	163
740502–740514	13	12,24	60E,55	220	65E,55	111
750328–750412	16	12,27	60E,50	251	60E,50	138
770402–770411	10	6,27	65E,50	257	60E,50	136
770424–770503	10	18,36	55E,55	272	65E,60	160
780318–780402	16	9,27	65E,55	240	65E,55	152
790429–790510	12	6,6	60E,55	322	60E,55	206

Table 2c

Ridges in the Asian region, summer season in the years 1946–1979.

Period	Days	$\delta\lambda,\Delta\lambda$	Position of ridges	Amplitude	Position of anomaly	Extreme value
510807–510905	30	12,24	45E,60	237	50E,60	176
540611–540620	10	12,24	40E,55	247	40E,55	173
570823–570908	17	9,12	60E,60	233	65E,60	197
580617–580626	10	9,30	60E,60	187	65E,60	134
630801–630810	10	9,12	125E,65	209	125E,60	158
640601–640613	13	15,27	40E,55	173	40E,50	94
700703–700714	12	9,18	130E,60	204	130E,60	167
710718–710729	12	9,30	55E,55	200	55E,55	171
720705–720716	12	6,12	40E,65	281	40E,65	233
770526–770609	15	6,27	70E,60	208	75E,60	181

Table 2d

Ridges in the Asian region, autumn season in the years 1946–1979.

Period	Days	$\delta\lambda,\Delta\lambda$	Position of ridges	Amplitude	Position of anomaly	Extreme value
491105–491114	10	9,27	45E,65	322	50E,65	230
491114–491125	12	9,15	40E,65	350	45E,65	280
541120–541204	15	12,21	45E,65	360	50E,65	290
581104–581115	12	9,30	40E,60	319	40E,65	208
591106–591115	10	12,24	50E,70	417	55E,70	358
601101–601111	11	9,12	55E,50	240	55E,50	145
630828–630908	12	6,12	45E,60	234	45E,60	170
671026–671111	17	9,36	55E,55	337	55E,55	254
740929–741021	23	6,15	60E,55	247	60E,55	206
791110–791123	14	12,12	60E,50	344	60E,55	233

Table 3

Ridges in the Pacific region in the years 1946–1980.

Period	Days	$\delta\lambda,\Delta\lambda$	Position of ridges	Amplitude	Position of anomaly	Extreme value
Winter season						
480114–480124	11	9,15	130W,50	338	135W,50	249
480202–480211	10	15,24	150W,60	329	155E,60	276
500103–500112	10	9,15	165W,50	312	170W,50	311
500113–500203	22	9,15	165W,60	441	170W,60	392
540112–540126	15	9,30	160W,60	306	170W,55	252
551214–551224	11	15,30	175W,60	389	180W,55	435
570107–570206	31	12,30	155W,60	362	155W,55	289
610118–610128	11	9,25	140W,65	357	130W,65	289
620107–620121	15	15,27	150W,60	363	150W,60	286
630112–630130	19	6,9	145W,60	394	145W,60	305
671224–680109	17	9,27	140W,50	323	145W,50	237
680206–680216	11	6,12	130W,60	361	130W,60	301
721201–721214	14	9,27	155W,60	340	155W,60	347
731231–740111	12	6,21	150W,60	444	155W,60	372
770116–770215	31	9,20	120W,50	187	115W,55	113
781230–790109	11	9,15	150W,70	415	145W,70	350
Spring season:						
630304–630313	10	9,24	145W,50	292	150W,50	235
650303–650315	13	9,30	130W,55	286	130W,55	236
670302–670312	11	12,30	155W,50	289	160W,50	266
Summer season:						
630810–630819	10	6,15	135W,60	198	135W,60	154
690607–690618	12	9,18	135W,65	194	135W,55	160
Autumn season:						
561119–561202	14	9,15	125W,50	309	125W,55	264
631011–631020	10	6,15	100W,55	241	95W,55	214
701117–701201	15	9,24	165W,50	318	170W,50	394
791104–791115	12	12,12	135W,55	266	140W,55	239

Table 4a

Troughs in the Pacific region, winter season for the years 1946–1980.

Period	Days	$\delta\lambda,\Delta\lambda$	Position of troughs	Amplitude	Position of anomaly	Extreme value
461130–461210	11	6,18	125E,45	−272	110E,50	−146
461211–461220*	10	24,24	150E,40	−241	155E,35	−97
470123–470207	16	18,36	150E,40	−232	165E,30	−88
480201–480212	12	12,18	145E,50	−221	145E,60	−86
490104–490130	27	9,27	155E,55	−217	170E,60	−111
491215–500114	31	12,30	140E,50	−339	140E,50	−118
501230–510109	11	6,21	155E,45	−315	170E,45	−111
510120–510209	21	9,36	155E,45	−255	170E,35	−53
511222–520101	11	9,18	140E,55	−269	145E,60	−103
520102–520123	21	15,30	135E,55	−308	135E,60	−155
520209–520312	33	18,27	150E,50	−292	145E,55	−94
521217–521228*	12	21,33	140E,50	−338	135E,40	−84
530114–530209*	27	21,36	160E,40	−292	170E,40	−105
530214–530305	20	15,24	155E,50	−271	155E,50	−70
531202–531214	13	15,30	165E,50	−253	170E,55	−129
540111–540128	18	9,15	140E,50	−319	130E,55	−147
540129–540212	15	15,27	175E,40	−269	170E,40	−168
541222–550112	22	12,27	150E,40	−282	160E,40	−107
550114–550129	16	12,21	155E,50	−319	170E,55	−160
550209–550225	17	15,30	145E,45	−250	120E,55	−50
560102–560116	15	6,6	130E,50	−273	115E,50	−121
560122–560213	23	12,36	140E,45	−305	135E,40	−107
560215–560226	12	12,27	135E,45	−245	125E,40	−90
561203–561220	18	12,24	140E,45	−287	160E,35	−136
561221–570102	13	12,21	170E,45	−350	180E,40	−228
570103–570113	11	9,15	145E,50	−317	140E,65	−148
570119–570128	10	12,30	150E,45	−213	165E,25	−50
570208–570223	16	15,36	145E,45	−255	115E,40	−80
571213–571224	12	12,33	130E,40	−170	120E,35	−53
571228–580106	10	18,33	150E,50	−291	165W,55	−168
580110–580119	10	15,24	180E,45	−272	165W,45	−186
580214–580225	12	12,30	170W,45	−293	160W,45	−264
581206–581217	12	3,15	175E,45	−303	175W,45	−201
581230–590117	19	6,15	130E,50	−328	120E,50	−165
590119–590129	11	9,15	165E,45	−290	175W,45	−105
591215–591225	11	6,21	150E,55	−300	125E,40	−51
591226–600104	10	12,21	155E,50	−347	165E,50	−138
600105–600114	10	6,18	140E,50	−304	120E,50	−96
600117–600129	13	12,36	155E,45	−340	155E,45	−104
600209–600305	26	12,30	150E,50	−275	150E,55	−104
601214–601224	11	15,21	170E,50	−318	175W,45	−185
610117–610129	13	12,36	175E,45	−337	170W,45	−216
610208–610304	25	12,36	150E,45	−283	150E,40	−72
611219–620118	28	15,30	160E,40	−268	165E,35	−127
620123–620209	18	15,36	170E,40	−306	175W,40	−172
620211–620314	31	15,24	145E,50	−347	145E,50	−149

Table 4a—*continued*

Period	Days	$\delta\lambda,\Delta\lambda$	Position of troughs	Amplitude	Position of anomaly	Extreme value
621214–621224	11	9,15	140E,55	−336	145E,55	−146
621231–630128	29	9,30	155E,40	−365	160E,40	−171
630201–630223	23	12,36	170E,40	−310	175W,40	−203
640117–640126	10	9,33	155E,50	−246	170E,65	−125
640127–640210	15	18,33	175E,45	−260	170W,75	−239
640211–640226	16	12,21	155E,45	−301	165E,50	−96
641206–641221	16	12,33	135E,50	−306	130E,55	−121
641226–650107	13	6,18	130E,55	−316	120E,60	−166
650110–650119	10	9,33	180E,45	−312	175W,45	−205
651204–651219	16	9,27	135E,50	−311	120E,60	−147
651228–660112	16	12,36	140E,45	−249	135E,40	−49
660113–660221	39	12,36	150E,50	−335	150E,50	−132
661124–661210	17	12,30	130E,50	−287	120E,50	−147
661226–670110	16	18,27	155E,45	−317	175W,55	−171
670114–670125	12	15,24	150E,50	−320	150E,65	−194
670130–670211	13	12,27	165E,45	−383	175E,45	−212
671129–671211	13	12,30	130E,45	−240	120E,40	−114
671224–680118	26	15,18	140E,45	−306	130E,45	−93
680119–680214	27	18,33	155E,40	−312	170E,35	−119
680215–680307	22	15,18	180E,40	−297	170W,40	−259
681219–690106	19	9,18	125E,45	−313	115E,50	−158
690109–690130	22	9,21	145E,50	−375	145E,55	−167
690206–690217	12	6,12	115E,60	−341	110E,60	−281
691205–691216	12	9,18	150E,55	−292	180E,55	−144
691225–700112	19	12,27	155E,45	−352	165E,45	−141
700126–700222	28	18,33	175E,45	−302	170W,50	−182
701123–701211	19	12,33	140E,45	−303	135E,45	−131
701214–701225	12	9,18	145E,50	−360	145E,50	−142
710131–710214	15	12,33	165E,40	−309	165E,35	−145
711124–711225	32	12,21	140E,45	−295	140E,45	−108
711226–720105	10	15,21	160E,55	−344	170E,55	−186
720110–720123	14	9,18	165E,45	−190	175E,35	−51
721230–730108	10	15,33	150E,60	−269	155E,65	−153
730131–730218	19	15,36	165E,45	−259	180E,50	−105
731228–740112	16	12,24	155E,45	−270	170E,35	−125
740115–740206	23	12,36	155E,40	−301	155E,40	−99
740221–740307	15	15,36	130E,50	−197	105E,45	−41
741219–750103	16	15,27	155E,50	−275	170E,50	−75
750104–750113	10	12,21	145E,45	−250	150E,35	−53
750124–750203	11	6,9	140E,50	−315	150E,65	−190
750209–750302	22	9,27	150E,45	−275	145E,40	−85
751204–751214	11	6,33	140E,50	−263	120E,45	−76
751215–751224	10	15,27	175E,50	−313	175W,50	−206
751225–760103	14	9,18	160E,45	−316	170E,40	−133
760105–760115	11	6,33	145E,45	−318	145E,45	−84
760119–760224	27	9,36	160E,45	−293	170E,40	−92
761128–761211	14	15,33	165E,45	−268	170E,45	−141

Table 4a—*continued*

Period	Days	$\delta\lambda,\Delta\lambda$	Position of troughs	Amplitude	Position of anomaly	Extreme value
761229–770214*	48	21,33	170E,45	−376	180W,45	−222
770206–770220	15	12,27	175E,45	−343	170W,45	−215
770221–770305	13	9,18	150E,50	−344	170W,55	−159
771203–771214	12	9,27	175E,40	−243	175W,40	−196
771217–771226	10	9,36	150E,50	−287	155E,65	−164
771227–780107	12	15,18	155E,50	−305	170W,45	−125
780108–780118	11	15,27	170E,45	−323	170W,45	−210
780121–780203	14	6,15	160E,45	−332	180E,40	−148
780219–780309	19	18,36	170E,40	−309	170W,40	−230
790102–790111	10	9,15	120E,60	−287	165W,40	−208
790112–790127	16	12,18	155E,50	−325	180W,60	−213
800114–800126	13	18,36	160E,45	−296	175W,60	−129
800206–800225	20	15,36	165E,45	−326	170W,40	−206

Table 4b

Troughs in the Pacific region, spring season in the years 1946–1980.

Period	Days	$\delta\lambda,\Delta\lambda$	Position of troughs	Amplitude	Position of anomaly	Extreme value
470310–470319	10	15,36	160E,45	−234	175W,40	−164
470501–470511	11	15,27	175E,50	−191	175E,50	−92
490227–490316	18	18,36	155E,55	−279	165E,55	−136
490315–490330	16	12,27	160E,50	−262	170E,50	−109
500516–500525	10	18,33	175E,50	−223	170E,50	−113
510227–510309	11	12,24	130E,55	−278	125E,60	−166
510322–510406	16	9,24	175E,55	−224	170W,55	−138
510512–510521	10	18,36	180E,50	−210	170E,45	−97
530414–530429	16	18,33	180E,50	−278	180W,50	−197
530526–530605	11	9,21	180E,50	−183	160E,45	−60
540429–540511	13	12,33	165E,55	−275	160E,60	−206
550310–550319	10	12,30	135E,55	−245	125E,60	−152
550510–550520	11	15,36	170W,55	−208	165W,55	−100
560331–560409	10	9,24	155E,50	−279	160E,55	−159
560513–560529	17	12,27	175W,55	−222	175W,55	−100
570306–570329	24	9,27	150E,45	−275	145E,40	−101
570508–570518	11	15,36	175W,50	−263	175W,45	−163
580226–580311	14	9,15	150E,50	−322	155E,55	−138
580325–580403*	10	21,33	150E,50	−287	160E,55	−136
580503–580516*	14	30,48	170E,50	−210	170E,50	−107
580518–580605	19	9,15	175E,50	−227	175E,50	−108
590223–590306	12	9,21	165E,45	−285	175E,45	−135
590310–590326	17	12,15	155E,40	−190	170E,40	−79
620315–620329	15	12,24	140E,45	−227	125E,40	−141
620503–620520	18	9,18	145E,45	−155	145E,45	−78
630225–630315	19	15,18	150E,40	−257	155E,40	−88
650222–650413	51	12,33	150E,45	−284	155E,40	−135

Table 4b—*continued*

Period	Days	$\delta\lambda,\Delta\lambda$	Position of troughs	Amplitude	Position of anomaly	Extreme value
650427–650506	10	9,21	140E,45	−220	140E,45	−106
660302–660322	21	15,30	130E,50	−259	115E,55	−155
660403–660413	11	12,33	145E,50	−275	180E,40	−182
660413–660424	12	6,27	160E,45	−224	160E,45	−137
670301–670406	37	15,27	145E,50	−255	140E,55	−106
690303–690327	23	15,30	155E,50	−271	165E,50	−98
700305–700316	12	12,30	175E,45	−345	170W,45	−277
700317–700402	17	9,27	160E,45	−320	160E,40	−173
710301–710319	19	18,33	150E,45	−241	155W,60	−170
710517–710610	25	9,21	175W,55	−225	175W,60	−132
720301–720319	19	12,36	170E,40	−268	180E,40	−195
730221–730329	37	9,36	145E,45	−287	145E,45	−94
740314–740327	14	18,33	170E,45	−341	180W,40	−268
750302–750312	11	6,15	160E,50	−299	165E,55	−157
760319–760411	24	12,27	175W,55	−234	170W,60	−165
760501–760511	11	12,24	170W,50	−242	170W,50	−144
770518–770604	18	6,33	155W,55	−191	145W,55	−118
780310–780325	16	15,27	145E,40	−209	125E,35	−68
780328–780413	17	12,18	155E,45	−238	155E,40	−140
790311–790324	14	15,27	155E,45	−268	170E,50	−111
790325–790403	10	9,18	155E,45	−245	160E,45	−94
790412–790428	17	9,36	140E,45	−201	140E,45	−94
790511–790525	15	18,30	180E,50	−215	180E,50	−98
800310–800329	20	12,33	160E,50	−278	170E,50	−127
800414–800424	11	9,9	165W,55	−299	160W,50	−234
800425–800512	18	15,33	175W,50	−260	175W,55	−119

Table 4c

Troughs in the Pacific region, summer season for the years 1946–1980.

Period	Days	$\delta\lambda,\Delta\lambda$	Position of troughs	Amplitude	Position of anomaly	Extreme value
490612–490621	10	18,24	155E,40	−121	170E,35	−72
490622–490703	12	9,33	150E,40	−103	160E,35	−40
500813–500823	11	9,18	175E,55	−177	170W,45	−150
510607–510617	11	9,12	170W,55	−212	165W,55	−110
510618–510702	15	12,15	165E,50	−154	160E,50	−95
520527–520615	20	18,30	175E,55	−174	155E,60	−93
540528–540614	18	15,30	170W,50	−242	160W,50	−119
540625–540709	15	12,18	170W,50	−183	170W,50	−133
550822–550901	11	12,36	175W,60	−175	175W,65	−132
560610–560622	13	18,27	165W,55	−185	160W,55	−106
560630–560711	12	9,15	125E,40	−104	115E,40	−49
570528–570607	11	18,27	170E,45	−150	145E,40	−66

Table 4c—*continued*

Period	Days	$\delta\lambda,\Delta\lambda$	Position of troughs	Amplitude	Position of anomaly	Extreme value
570608–570617	10	15,30	180W,45	−190	160W,45	−98
570620–570629	10	12,21	165E,45	−202	165E,45	−128
580614–580624	11	6,15	180E,50	−172	175W,45	−89
630528–630608	12	15,27	170E,45	−215	170E,45	−108
650523–650612	21	12,36	175E,50	−307	170E,50	−187
650630–650713	14	12,27	155E,45	−123	160E,45	−74
660615–660701	17	15,36	155W,50	−195	150W,50	−152
670606-670626*	21	21,27	175E,50	−145	165E,50	−53
680629–680712	14	12,18	160E,45	−168	165E,45	−120
690602–690613	12	12,18	180E,50	−239	170E,55	−124
690813–690828	16	9,24	125E,45	−139	125E,45	−110
700528–700610	14	12,36	170W,45	−195	160W,45	−101
720611–720625	15	15,30	175E,55	−179	175E,55	−105
720708–720719	12	9,30	175E,50	−153	170E,50	−114
730528–730606	10	12,21	170W,55	−215	170W,60	−108
730607–730617	11	12,30	155W,50	−192	140W,50	−128
760714–760725	12	15,33	165W,50	−156	160W,50	−129
770608–770625	18	9,36	175W,50	−160	170W,50	−62
790703–790717	15	9,24	130E,40	−119	135E,45	−60

Table 4d

Troughs in the Pacific region, autumn season for the years 1946–1979.

Period	Days	$\delta\lambda,\Delta\lambda$	Position of troughs	Amplitude	Position of anomaly	Extreme value
471108–471120	13	18,36	150E,45	−246	160E,40	−123
491121–491202	12	9,12	170W,50	−305	165W,50	−227
501120–501129	10	9,21	120E,50	−227	110E,50	−129
511014–511025*	12	21,36	160E,50	−222	155E,50	−126
511026–511108	14	12,33	170E,50	−284	170E,50	−147
531004–531019*	16	30,33	170W,55	−261	165W,55	−154
531109–531124	16	9,33	155E,50	−302	155E,50	−129
541004–541013	10	15,27	145E,45	−166	140E,45	−96
541015–541024	10	12,33	165W,50	−224	160W,50	−116
541104–541114	11	15,36	155E,50	−269	180E,45	−125
541115–541124	10	6,12	175W,45	−352	170W,45	−270
561116–561128	13	9,33	165E,50	−312	175E,45	−183
570831–570912	13	12,36	175W,50	−181	175W,50	−124
571025–571103	10	9,18	180E,50	−216	175W,50	−119
591006–591024	19	18,27	175E,45	−231	175E,40	−174
591111–591202	22	12,27	170E,50	−312	175E,50	−180
601126–601205	10	12,36	140E,55	−352	145E,55	−203
621022–621104	14	9,15	175W,50	−267	175W,45	−180

Table 4d—*continued*

Period	Days	$\delta\lambda,\Delta\lambda$	Position of troughs	Amplitude	Position of anomaly	Extreme value
621113–621125	13	15,27	175E,50	−322	175W,50	−196
630904–630913	10	3,9	175W,50	−241	180W,45	−179
630914–630927	14	12,36	145E,45	−141	140E,40	−83
641118–641128	11	9,33	145E,45	−246	150E,40	−110
651105–651118	14	12,24	145E,55	−337	140E,55	−185
661110–661121	12	9,27	125E,55	−305	120E,55	−183
670908–670929	22	15,30	170W,50	−241	165W,50	−173
671023–671103	12	12,30	175E,50	−256	175E,50	−126
671111–671126	16	18,30	160E,50	−299	160E,45	−149
681028–681108	12	9,30	165W,50	−296	160W,45	−196
691123–691207	15	9,21	175W,50	−356	170W,50	−278
710915–710925	11	12,36	170E,55	−115	140E,70	−98
711111–711122	12	15,15	170E,55	−269	175E,55	−133
721101–721113	13	9,27	150E,50	−271	145E,55	−126
721124–721204	11	9,36	150E,45	−200	155E,40	−83
731109–731217	39	9,33	140E,45	−273	135E,45	−109
781118–781127	10	9,36	160E,45	−246	165E,45	−104
790921–791017	27	15,30	180E,50	−262	180E,50	−169
791028–791109	13	12,21	155E,50	−285	155E,50	−153
791111–791123	13	6,9	125E,50	−237	115E,45	−122

Table 5a

Troughs in the Atlantic region, winter season for the years 1946–1980.

Period	Days	$\delta\lambda,\Delta\lambda$	Position of troughs	Amplitude	Position of anomaly	Extreme value
480204–480216	13	15,24	70W,60	−365	55W,60	−252
531225–540103	10	3,18	85W,65	−415	85W,65	−323
560129–560211	14	9,21	70W,65	−356	65W,65	−232
570110–570121	12	9,36	75W,60	−361	80W,60	−220
570124–570202	10	12,36	60W,60	−385	35W,60	−303
590123–590227	36	15,33	65W,60	−327	60W,60	−196
610118–610201	15	6,12	65W,50	−358	60W,50	−251
620127–620205	10	6,12	70W,55	−363	70W,55	−199
630112–630201	21	12,30	80W,60	−370	85W,55	−228
650130–650213	15	15,15	80W,60	−312	85W,60	−173
680214–680223	10	6,9	70W,50	−409	65W,50	−295
700214–700228	15	9,21	75W,60	−325	75W,60	−180
721130–721209	10	18,36	85W,60	−368	90E,60	−311
721211–721220	10	9,12	55W,55	−336	45W,50	−283
730109–730118	10	9,21	55W,55	−347	45W,55	−279
770127–770205	10	12,27	70W,50	−335	70W,45	−213
790128–790208	12	9,36	70W,40	−227	60W,40	−203
790209–790219	11	6,12	50W,50	−221	40W,50	−304

Table 5b

Troughs in the Atlantic region, spring season for the years 1946–1980.

Period	Days	$\delta\lambda,\Delta\lambda$	Position of troughs	Amplitude	Position of anomaly	Extreme value
540326–540404	10	12,27	80W,55	−342	85W,55	−283
540406–540415	10	6,15	60W,60	−267	60W,60	−211
610330–610414	16	6,15	65W,45	−217	65W,40	−161
620418–620429	12	9,21	65W,55	−257	60W,60	−204
630220–630310	19	9,30	65W,55	−333	55W,55	−227
630405–630415	11	9,33	55W,45	−223	45W,40	−205
640222–640310	18	6,18	85W,65	−449	85W,65	−331
640227–640327	30	9,27	80W,65	−315	85W,70	−222
640403–640413	11	9,36	15E,35	−130	10E,40	−82
660327–660407	12	6,15	70W,45	−273	70W,40	−205
670502–670512	11	12,30	95W,55	−154	100W,55	−175
680516–680528	13	6,30	55W,50	−179	55W,45	−166
690306–690317	12	9,33	60W,40	−268	55W,40	−242
700325–700405	12	6,15	80W,50	−256	85W,55	−191
700522–700605	15	9,30	55W,60	−228	40W,65	−183
740318–740330	13	9,33	75W,60	−337	75W,60	−256
760313–760323	11	9,15	70W,65	−425	70W,65	−332

Table 5c

Troughs in the Atlantic region, summer season, for the years 1946–1979.

Period	Days	$\delta\lambda,\Delta\lambda$	Position of troughs	Amplitude	Position of anomaly	Extreme value
470821–470901	12	12,15	60W,60	−190	60W,60	−107
500804–500813	10	9,18	35W,60	−172	35W,60	−107
510707–510717	11	9,15	80W,65	−211	85W,60	−142
550629–550713	15	12,24	50W,65	−214	50W,65	−141
580606–580620	15	6,18	70W,55	−228	70W,50	−176
640526–640609*	15	27,33	50W,50	−173	45W,50	−141
660530–660610	12	12,36	50W,60	−166	40W,65	−107
660603–660614	12	18,24	50W,60	−216	45W,65	−155
680730–680812	14	6,12	75W,60	−272	75W,60	−199
690623–690706	14	9,30	60W,60	−228	60W,60	−149
690720–690805	17	9,18	35W,60	−196	35W,60	−141
720821–720830	10	9,15	60W,65	−242	60W,70	−167
780531–780613	14	12,30	70W,65	−270	65W,65	−191

Table 5d
Troughs in the Atlantic region, autumn season for the years 1946–1980.

Period	Days	$\delta\lambda,\Delta\lambda$	Position of troughs	Amplitude	Position of anomaly	Extreme value
491024–491104	12	18,27	70W,60	−227	70W,60	−182
620922–621002	11	12,36	35W,60	−201	30W,60	−165
691015–691029	15	12,30	65W,60	−285	70W,60	−212
721010–721020	11	12,18	75W,60	−284	80W,60	−240
740909–740919	11	18,27	65W,60	−290	70W,60	−179

* In addition to the events that fulfil the criteria mentioned in Chapter 3, ten more troughs (marked with * in Tables 4 and 5) are included. These events have a shift in the position of maximum amplitude by more than 18 degrees longitude per day. Otherwise two of these events could be divided in two events each, a third one would be shortened by three days (from 21 to 18 days). For all of the ten events, the trough at 10° north or south of the actual latitude, even though it does not fulfil the amplitude criteria, has a shift in the position of less than 18 days per day.

Table 6
Average ratio (A) between amplitude given relative to climatological and zonal average field, respectively. The standard deviation of A is given by σ. The results are given for MST events.

	Region			
	Pacific		Atlantic	
Season	A	σ	A	σ
Winter	0.49	0.17	0.74	0.12
Spring	0.57	0.15	0.78	0.13
Summer	0.66	0.18	0.73	0.09
Autumn	0.59	0.15	0.79	0.06

compare the positions found for the MSR and MST events throughout the year with the normal positions of ridges and troughs.

Figure 2 shows that the standard deviation of $\sigma(\varphi)$ given in eq. (4) varies slowly with time, with a maximum in January and a minimum in July. Thus we may characterize the main features of these seasons by showing the conditions for one month, for instance January and July. It is interesting to note that the decrease in the standard deviation during the spring season is slower than the increase of the same quantity during the fall season. But even with these rather large changes in the standard deviation during the spring and fall season, we may still characterize some features of these seasons by giving the conditions for April and October, respectively.

In Fig. 3a–d, the difference between the climatological field and the zonally averaged climatological field for January, April, July and October is shown. A comparison between these deviation patterns and the tabulated positions of ridges and troughs shows that the positions of the events coincide by and large with the normal position of ridges and troughs. This may also be

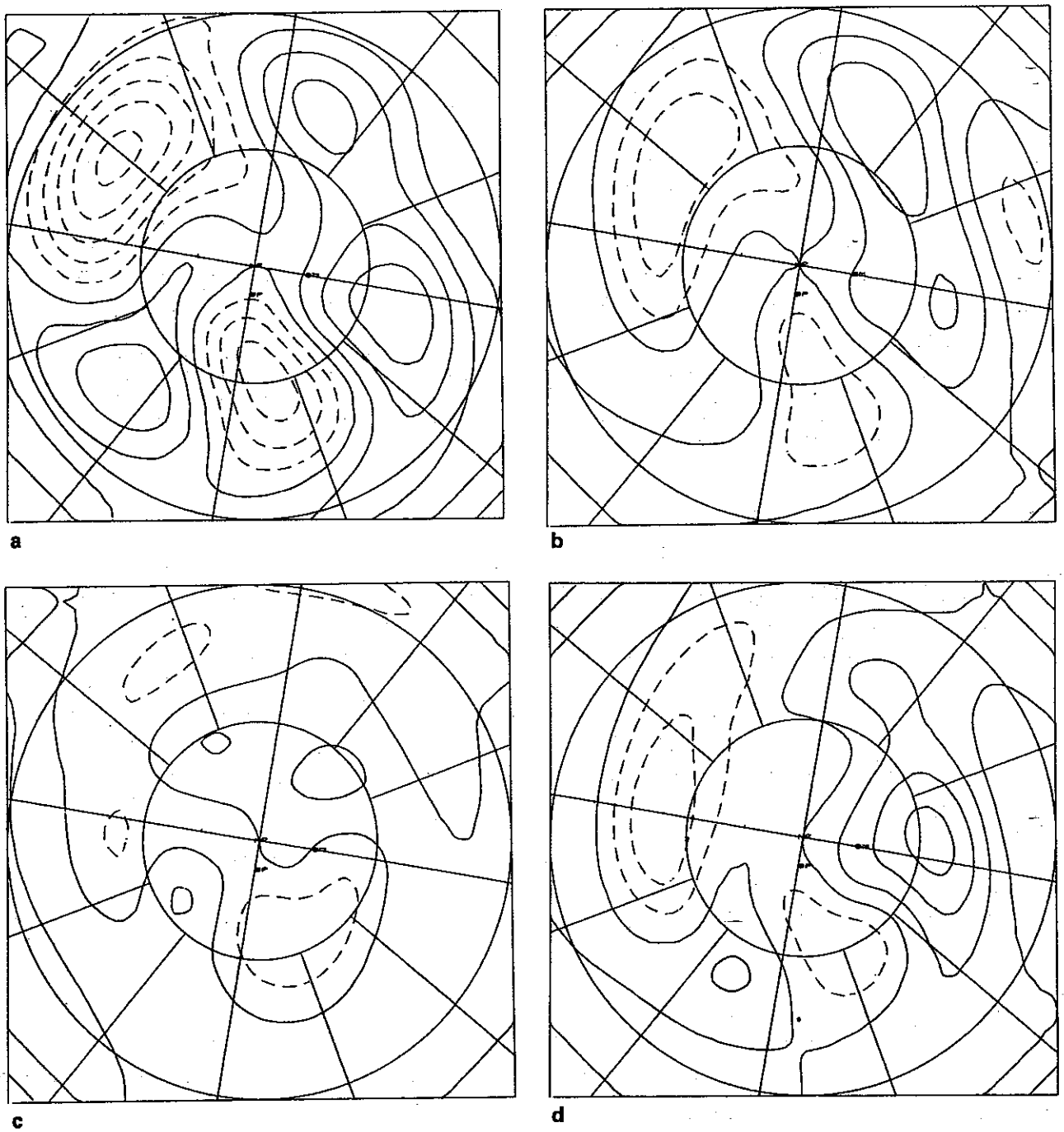

Fig. 3. The difference between the monthly climatological mean field and the monthly zonal mean field for the period 1946–1979. Contour interval 40 m. The zero and positive contours are solid, and negative ones are dashed. a) January; b) April; c) July; d) October. Stereographic map. Latitudes and longitudes are drawn every 30°. The line from the pole pointing to the right is the Greenwich Meridian.

manifested by computing the ratio between the amplitudes given in columns seven and five in Tables 1–5. In all cases except four, these ratios are less than unity. Both the MSR and MST events (Table 6) may thus be characterized as being largely an amplification of the normal pattern.

To illustrate the type of $\bar{z}^*(\lambda, \varphi)$ fields obtained, a typical MSR event for each season is shown in Fig. 4a–d. It turns out

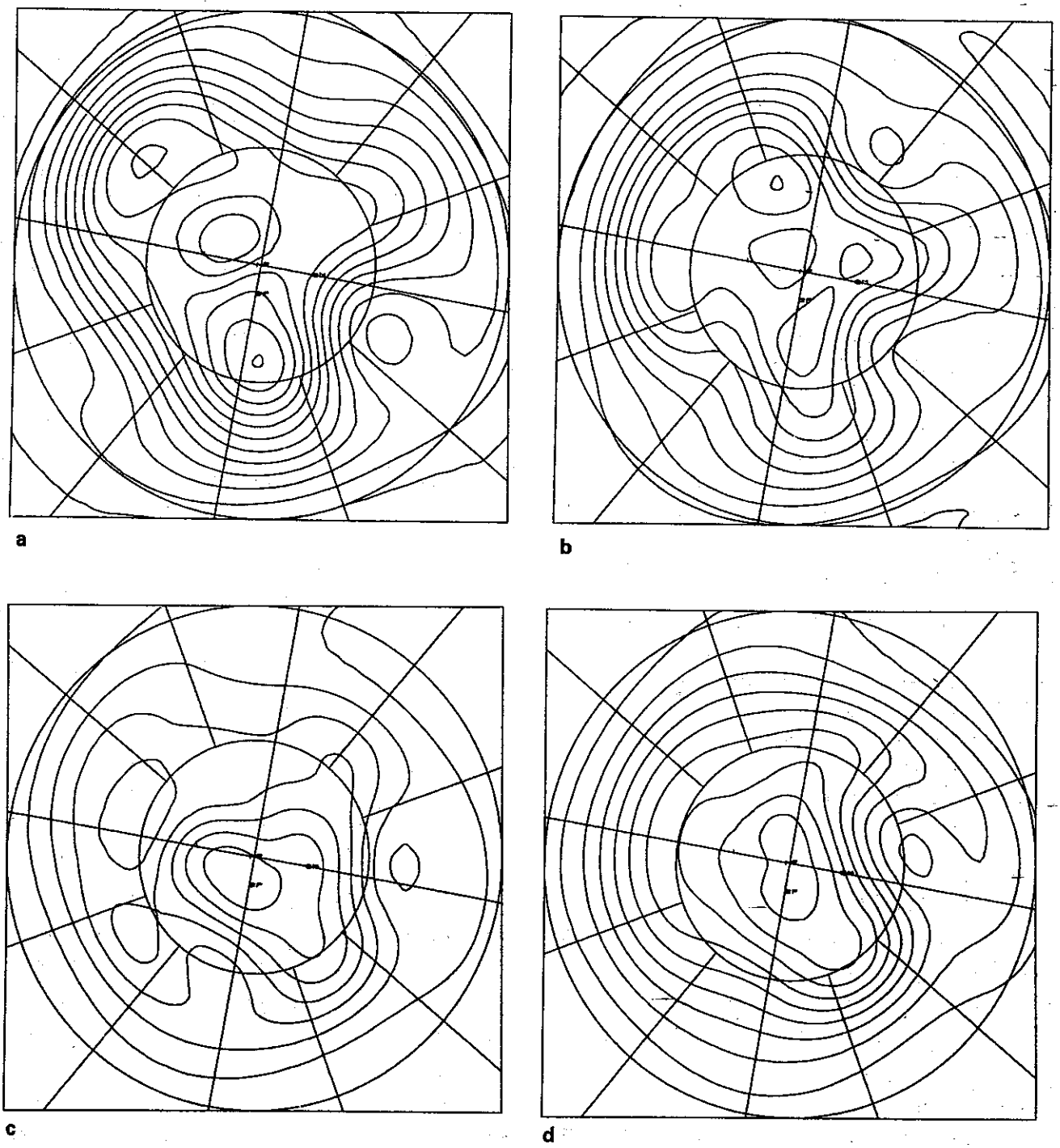

Fig. 4. Examples of typical MSR events for the four seasons. Contour interval 80 m. a) Feb. 1–15, 1965; b) April 6–19, 1973; c) June 24–July 3, 1976; d) Sep. 29–Oct. 17, 1951.

that by the chosen restrictions on amplitude and stationarity, the averaged picture of the ridges (and troughs) nearly always has a closed contour line, i.e. there is a local negative zonal index.

Overlap between ridges and troughs

As seen from Tables 7 and 8, we have identified 281 troughs and 229 ridges, which amount to 4323 and 3270 days, respectively. Together this should amount to 7593 days,

Table 7
The number of days and MSR events for the period 1946–1980 together with the average positions.

Season	Year	Winter	Spring	Summer	Autumn
Number of days	3270	1354	816	275	825
Number of MSR events	229	91	61	21	56
Number of days pr. event	14.3	14.9	13.4	13.1	14.7
Number of days pr. season	95.1	39.1	23.3	8.1	24.3
Relative number of days (%)	26.0	43.3	25.3	8.8	26.7
Number of events pr. season	6.7	2.6	1.7	0.6	1.6
Relative number of events in the Pacific	10	17.6	4.9	9.5	7.1
Relative number of events in the Atlantic–Europe	66.9	74.7	52.5	42.9	75
Relative number of events in Asia	23.1	7.7	42.6	47.5	17.9
Average position in the Pacific (°W)	137.5	147.8	140.0	132.5	131.3
Average position in the Atlantic–Europe (°E)	0	−3.9	2.3	18.9	1.4
Average position in Asia (°E)	60.2	67.1	59.0	68.0	50.5

or on the average 220.8 days per year. However, as may be seen by comparing Tables 1–5, there is to some extent an overlap between ridges and troughs. Taking all degrees of overlap (even only one day) into account, we have found 1391 days with overlap. As regards the number of events, there is partly overlap between 136 MSR and 156 MST events. Consequently, the real number of days included in the events may be reduced from 7593 to 6202 days, which on the average corresponds to 180.3 days per year.

Seasonal and longitudinal variation

The distributions of the events as function of the month and longitude are given in Tables 9 and 10. The occurrence of MSR events (Table 9, right hand column) varies considerably through the year. They are most frequent in winter (December and January), and relatively few in the summer and early autumn (June–September). However, if we look at the Asian region separately, we find a quite different distribution. A marked maximum is found in spring (April and May), and also a maximum in late autumn (November).

Most of the MSR events are located in the Atlantic–European region. The average position of these events is at 0° longitude. In the Pacific region the average position of the events is found to be at 138° W.

Annual distribution

In Figs. 5 and 6 the annual distributions of MSR and MST events are shown. Regarding

Table 8
The number of days and MST events for the period 1946–80 together with the average positions.

Season	Year	Winter	Spring	Summer	Autumn
Number of days	4323	2024	1109	595	595
Number of MST events	281	124	70	44	43
Number of days pr. event	15.4	16.3	15.8	13.5	13.8
Number of days pr. season	125.7	58.4	31.7	17.5	17.5
Relative number of days (%)	34.4	64.7	31.9	19.0	19.2
Number of events pr. season	8.2	3.6	2.0	1.3	1.3
Relative number of events in the Pacific	81.8	85.5	75.7	70.5	88.4
Relative number of events in the Atlantic	18.2	14.5	24.3	29.5	11.6
Average position in the Pacific (°E)	158.8	151.8	161.4	170.5	165.4
Average position in the Atlantic (°W)	64.0	67.8	66.7	57.5	57.4

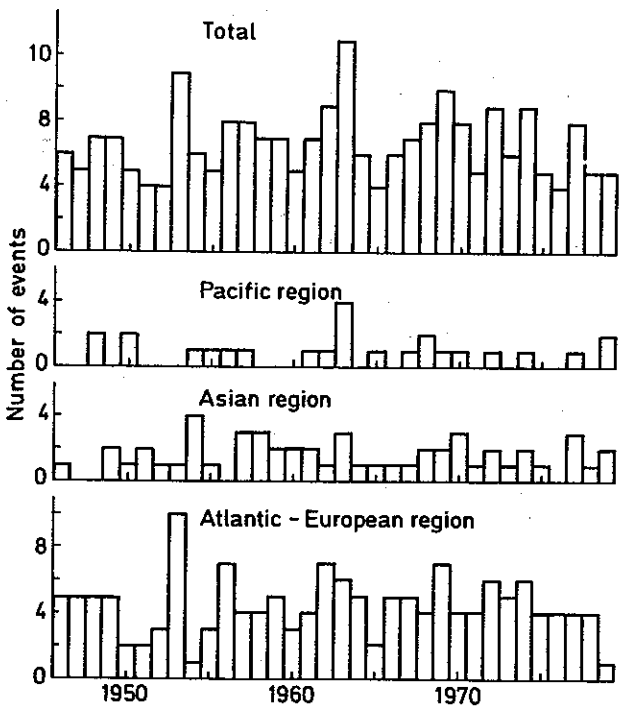

Fig. 5. Annual frequencies of MSR events.

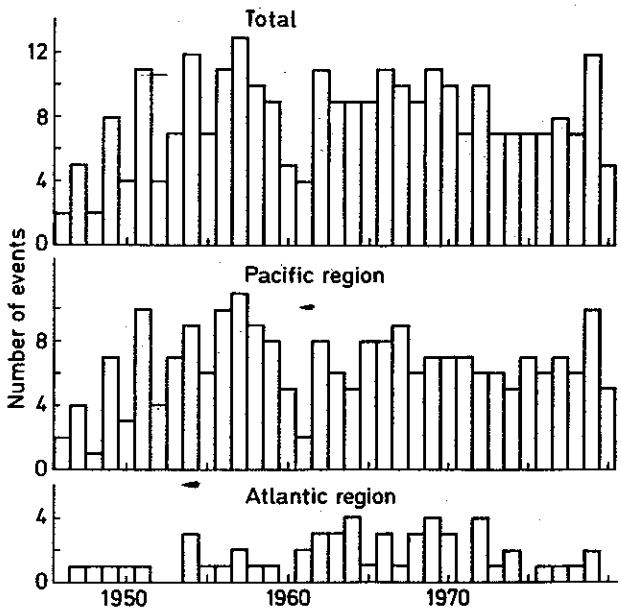

Fig. 6. Annual frequencies of MST events.

Table 9

Number of MSR events as function of season and longitude.

	Pacific region Degree west									Atlantic–European region											Asian region Degree east						Sum
	180	170	160	150	140	130	120	110	100	30	20	10	0	10	20	30	40	50	60	70	80	90	100	110	120	130	
J		2	2	4	2	1	1				6	5	2	4	2	2		1		1	1						36
F				1		1				1	7	4	4	4	1					1							24
M			1	1		1					3	8	6	2	1	1		2	1	1							28
A												1	2	3				6	5	1							18
M												1		2	1	3	2	2	2	2							15
J					1								2		2	1	2		1	1							10
J												1					1	1								1	4
A					1									1	2		1		1						1		7
S												2	1	2			1										6
O									1	1	2	5	3	7	3				1								23
N		1				1	1			1	3	4	6	1	1		4	3	1								27
D	1		1							4	10	3	5	2	1	1		1	2								31
	1	3	4	6	5	4	1		1	7	31	34	31	28	14	8	11	16	14	7	1				1	1	229

Table 10

Number of MST events as a function of season and longitude.

	Atlantic region Degree west									Pacific region Degree east										Sum
	100	90	80	70	60	50	40	0	−10	110	120	130	140	150	160	170	180	190	200	
J			2	3	2						1	4	9	19	6	4	2			52
F			2	5		1				1		2	5	9	5	6	1	1		38
M		1	4	2	1							3	4	11	6	7				39
A				3	2				1				2	2	1	1	1	1		14
M	1				2								2	1	1	2	4	4		17
J				2	1	3								2	2	6	4	5	2	27
J			1			1	1				1	1		1	1	1		2		10
A			1		2		1				1					1	1			7
S				1			1						1			2	1	1		7
O			1	2									1		2	3	3	1		13
N											3		4	6	3	3	2	2		23
D		2			1						2	5	9	6	4	5				34
Sum	1	3	11	18	11	5	3		1	1	8	15	37	57	31	41	19	17	2	281

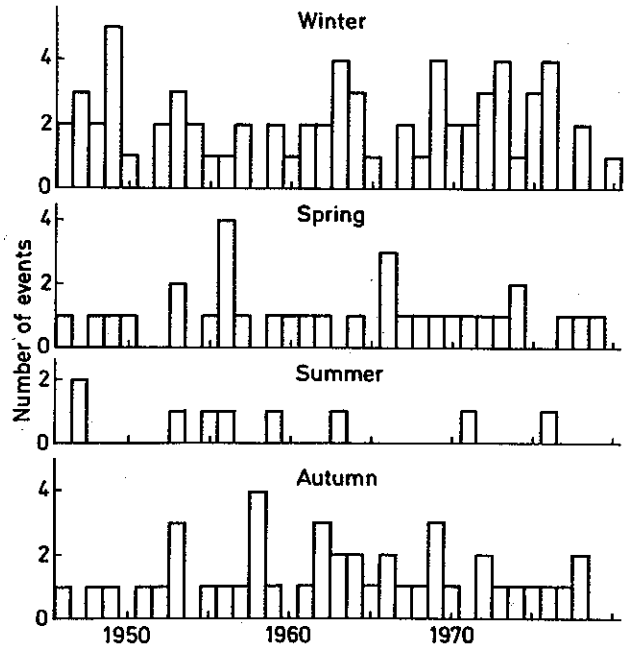

Fig. 7. Annual frequencies of MSR events for each season in the Atlantic-European region.

the troughs, the number of events each year increases during the first nine years from 1946, having a maximum occurrence in the late fifties. This trend is most pronounced for the Pacific region. For the MSR events, the trend is much weaker.

The number of MSR events in the Atlantic–European region and of MST events in the Pacific region is so large that it may be of some interest to study the seasonal variation of these events (Figs. 7 and 8). As seen from these figures, MST events are observed in all winter seasons. For the Atlantic-European region, however, we find five winter seasons without MSR events. Taking the MSR events observed in the two other sectors into account, only one winter season (1957–58) is lacking MSR events.

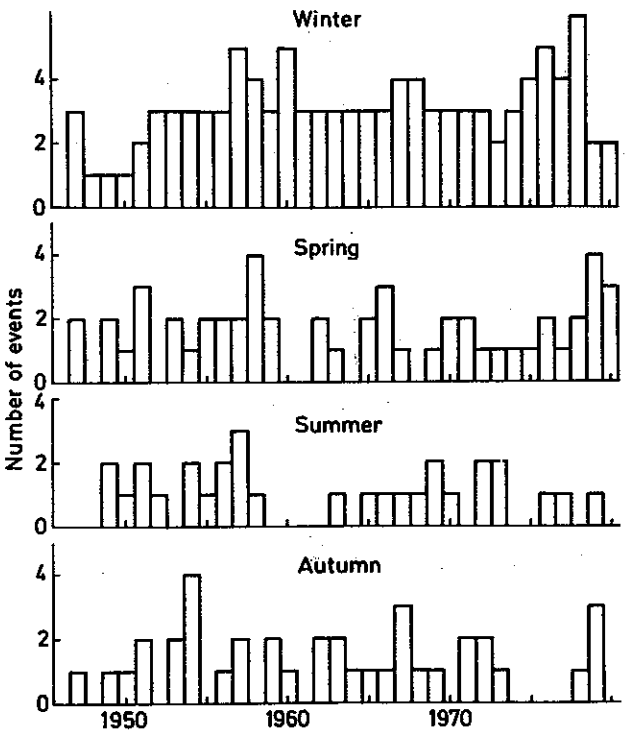

Fig. 8. As Fig. 7 for MST events in the Pacific region.

Major stationary events as function of the latitude

Figure 9 gives the distribution as a function of latitude of maximum amplitude. The latitude is found by searching for maximum deviation between the average field for the events and the climatological zonal average field. As mentioned above, the events are localized from Hovmøller diagrams at 50 and 60° N, and at 40, 50 and 60° N for ridges and troughs, respectively. A study of the 500 mb field indicates that a few more events could be found by analysing the Hovmøller diagrams at 70° N.

As seen from Fig. 9, the variation in latitude is greater for events in the Atlantic than in the Pacific region. The average values for the latitudes are about 56° N for all regions except for the MST events in the Pacific region, being situated at about 48° N.

The duration of the events and variation in the amplitude

In Fig. 10 the distribution of the amplitudes for all 4 seasons is given. For the MST events, the spread in amplitude is larger for the Atlantic than for the Pacific region, but the opposite is the case for the ridges. Concerning the troughs, the average amplitude

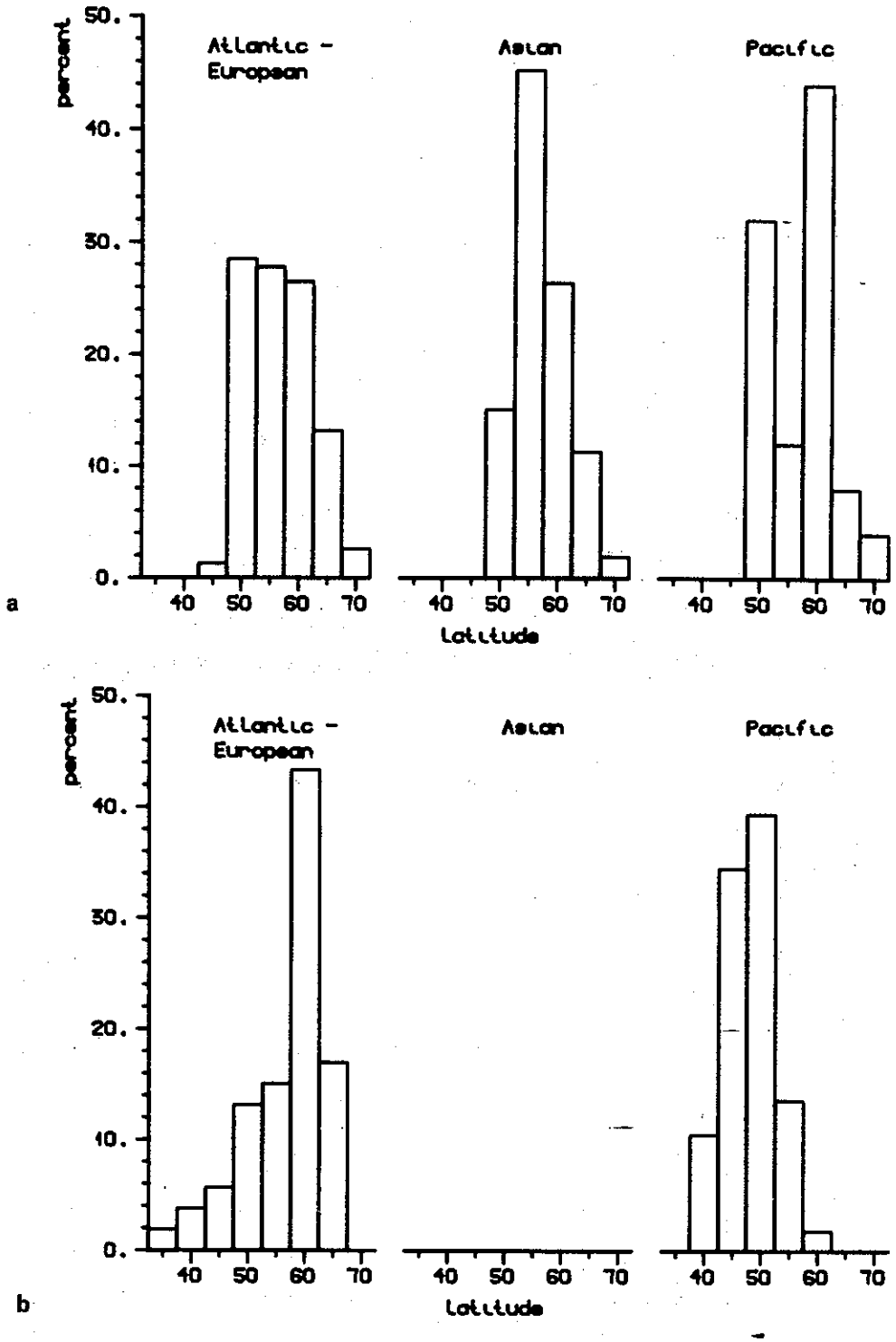

Fig. 9. The distribution of a) MSR and b) MST events as function of latitude.

is largest in the Atlantic region. In the case of ridges, however, the mean amplitude is greatest in the Pacific region and smallest in the Asian region. Except for the Asian region, the mean amplitude for the ridges is larger than for the troughs.

The distribution of the duration of the events is given in Fig. 11. The distribution for ridges and troughs is very similar, and the average lengths of the events are calculated to 14.3 and 15.4 days for ridges and troughs, respectively. Using first order Mar-

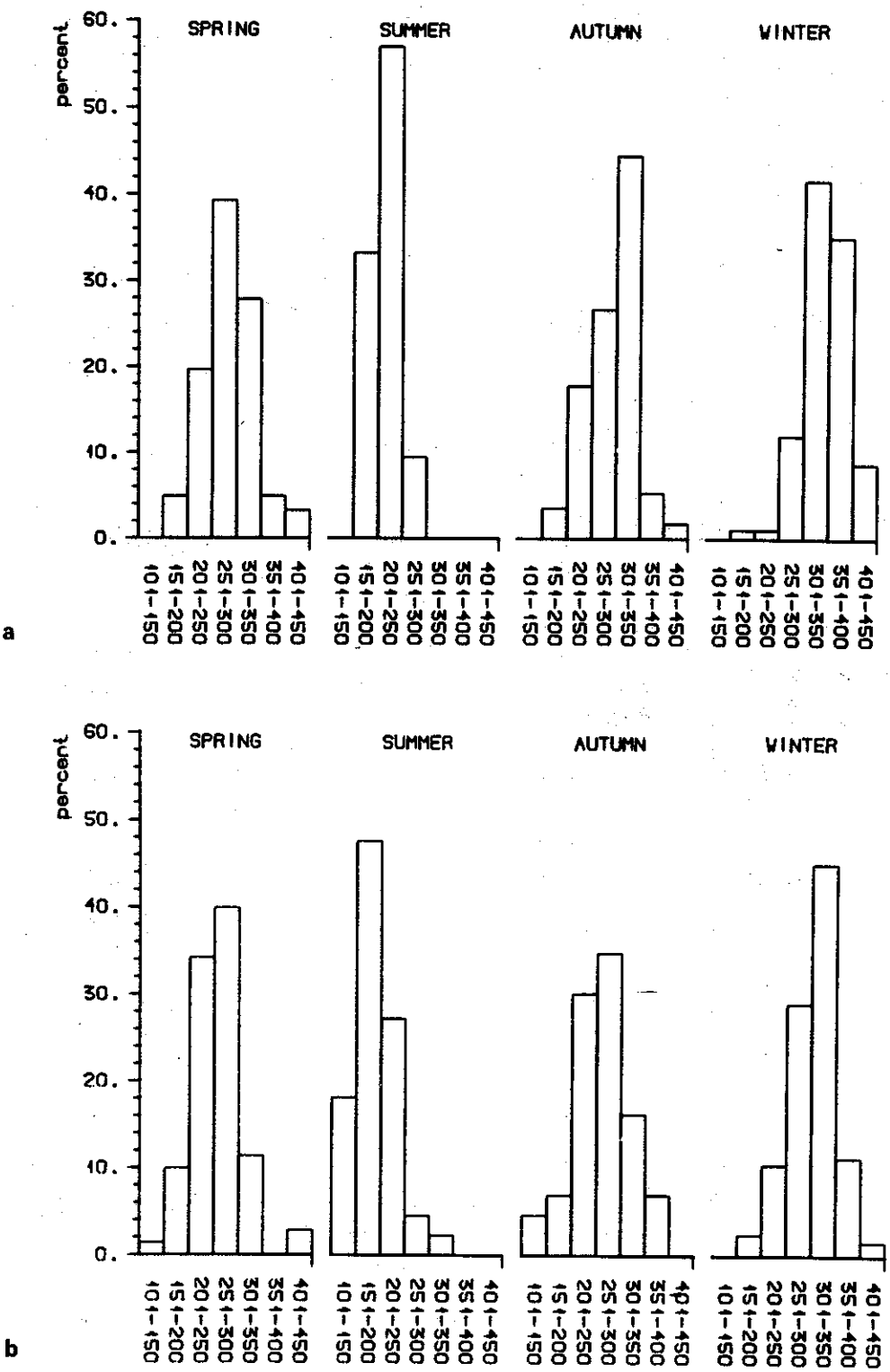

Fig. 10. The distribution of a) MSR and b) MST events as function of the amplitudes. The length of the interval for grouping the events according to the amplitude is chosen equal to 50 m.

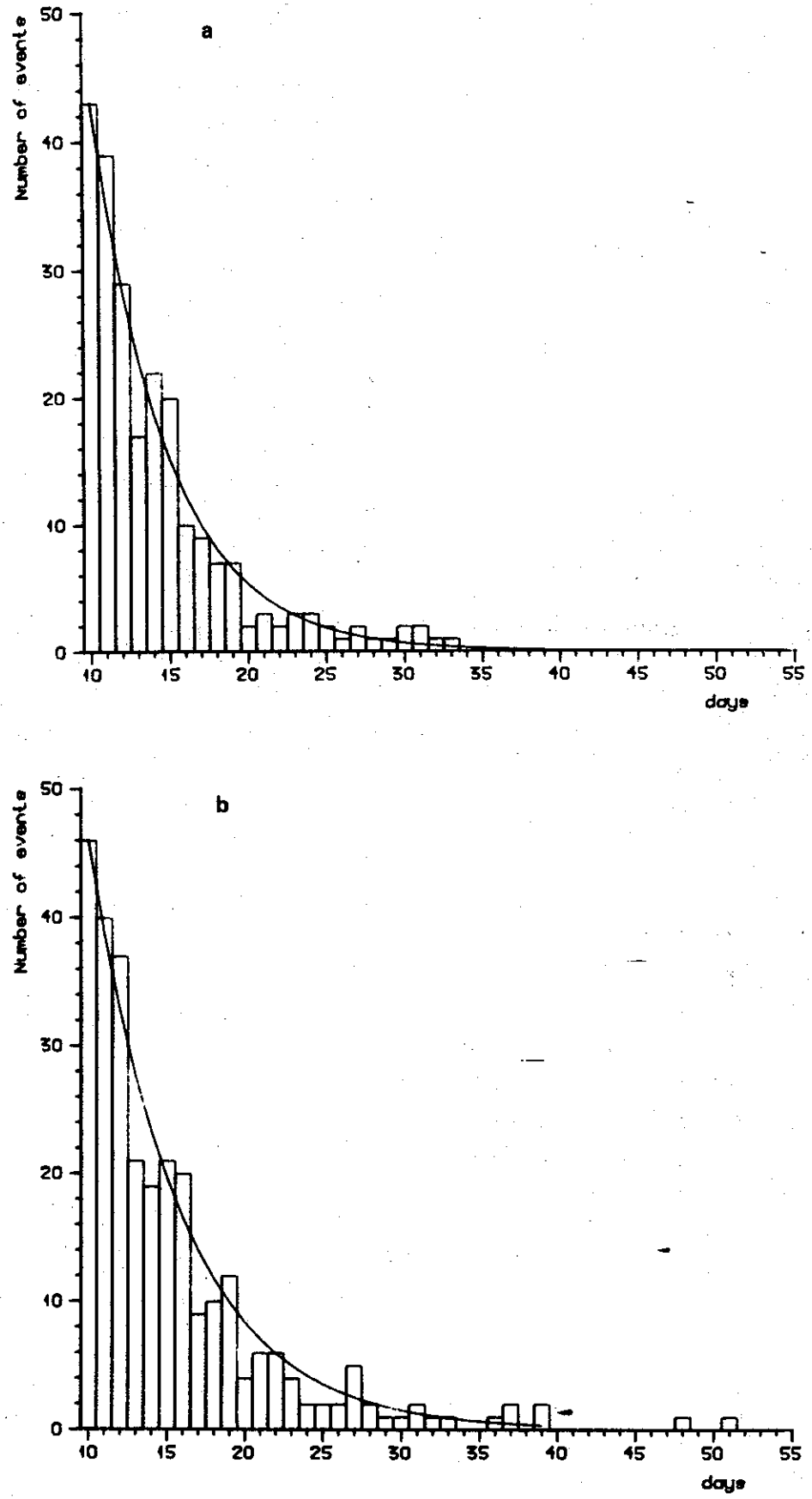

Fig. 11. The distribution of the duration of a) MSR and b) MST events. The Markov curves are normalized to fit the 10-days events.

kov chain the conditional probability, P_{11}, for having an event when it occurred the day before, is given by

$$ED = \frac{1}{1 - P_{11}}$$

where ED is the average length of the events. The probability P for an event to last for n days is given by

$$P = P_{11}^{n-1}(1 - P_{11}).$$

As seen from Fig. 11, the distribution can approximately be reproduced by first order Markov chain with $P_{11} = 0.811$ and $P_{11} = 0.843$ for ridges and troughs, respectively.

This result is rather disappointing, since it causes difficulties in estimating the duration of the events in advance. As seen from Fig. 11, a possible preferred persistence of MST events is from 13 to 16 days. However, tests show that this is of no statistical significance. The level of significance for having a flat curve from 13 to 16 days is as high as 13%.

5. SOME TYPICAL ANOMALY PATTERNS ASSOCIATED WITH THE MSR EVENTS

The phenomena of blocking have lately been linked with the existence of large persistent positive anomalies of the 500 mb winter circulation, Dole (1983) and Charney et al. (1981). But persistence of an anomaly by itself does not guarantee the persistence of a ridge. However, Charney et al. examined each of the 14 anomaly events found in their data, and in each case a pronounced ridge was indeed present.

We have computed the anomaly pattern associated with each MSR and MST event. In Tables 1–3 the extreme values of the anomaly associated with the MSR events are given. For the winter season we usually find anomalies exceeding 200 m. In the Atlantic–European region, Table 1a, only 3 out of 68 events have an anomaly less than 150 m. In the Pacific region, Table 3, 1 of 16 winter events has an anomaly less than 200 m.

The anomaly patterns found show a rather large variety. However, some patterns are typical for each season. We will here focus on a few examples from the Atlantic–European and the Asian region. For the winter season the event occurring from February 1 to February 15, 1965 is shown in Fig. 4a as a typical example. The MSR is located at 20° west of the 'normal' position. The anomaly pattern for this event, given in Fig. 12a, is rather similar to the Eastern Atlantic anomaly which Wallace and Gutzler (1981) called positive pattern index.

An example of the anomaly pattern for an MSR event localized about 10° to the east of the 'normal' position is given in Fig. 12b. This anomaly resembles more the Eastern Atlantic anomaly with a negative pattern index. For the MSR events having a 'normal' position about Greenwich, the anomalies are usually somewhat smaller in value.

A typical MSR event in the spring season, April 6 to April 19, 1973, is shown in Fig.

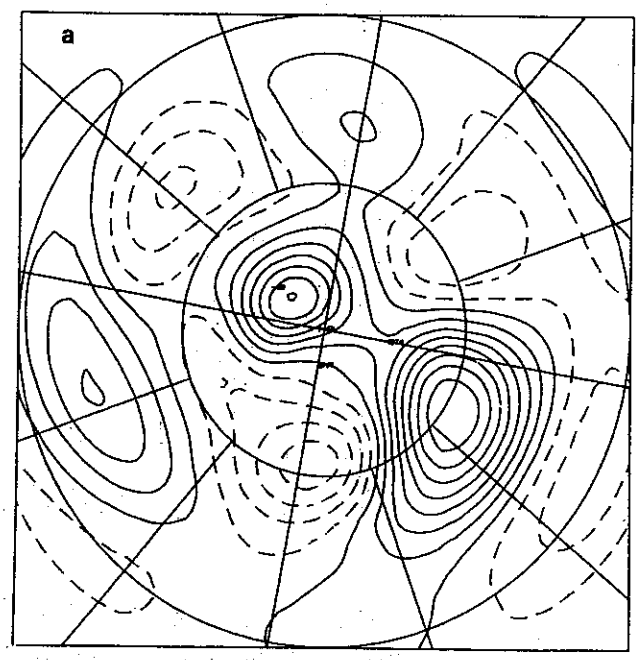

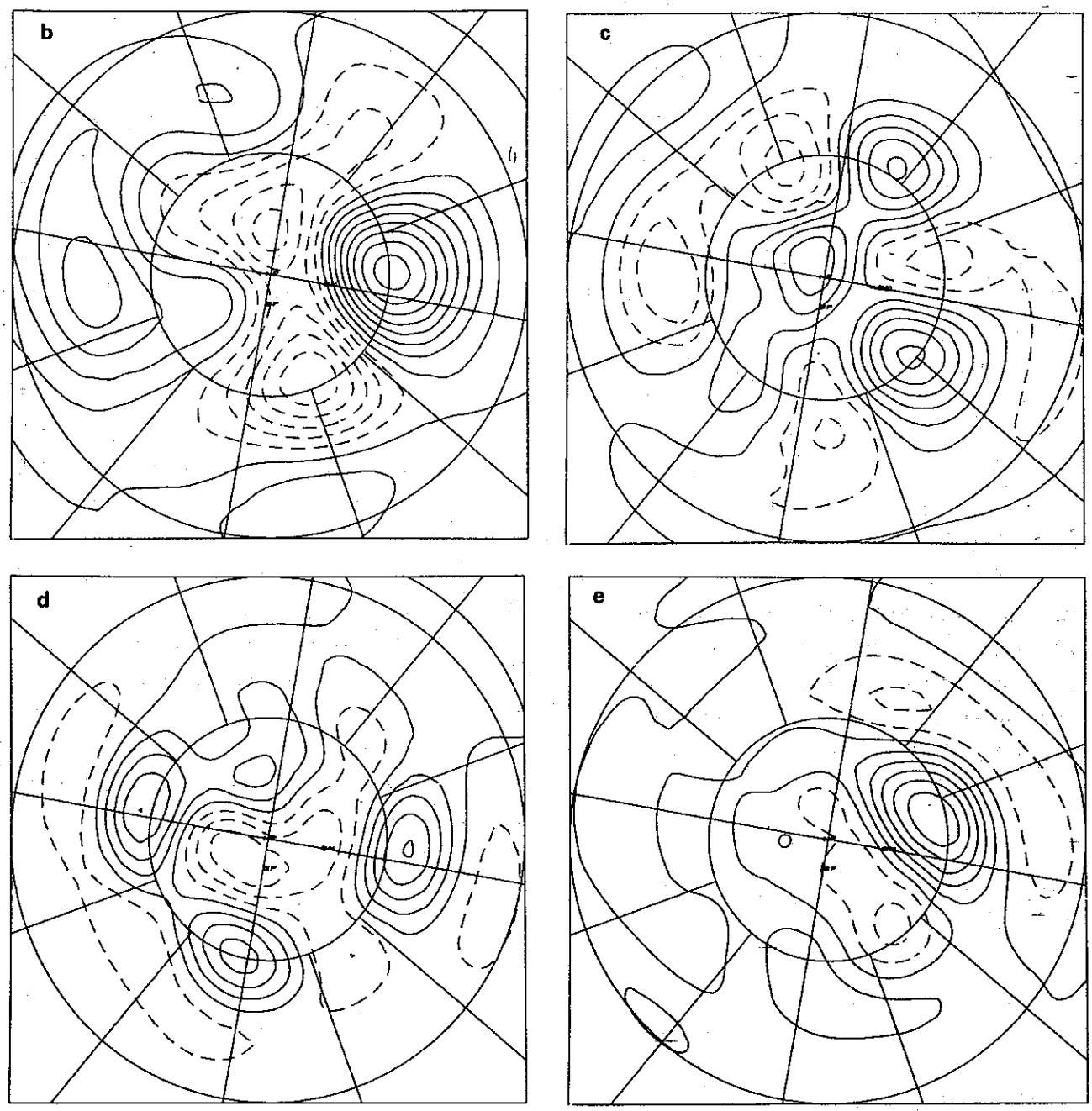

Fig. 12. Some examples of typical deviation (anomaly) between the average field for MSR events and the corresponding month climatological mean field. Contour interval 40 m. The zero and positive contours are solid, and the negative ones are dashed. a) Feb. 1–15, 1965; b) Jan. 26–Feb. 15, 1959; c) Apr. 6–19, 1973; d) June 24–July 3, 1976; e) Sept. 29–Oct. 17, 1951.

4b, and the anomaly pattern for this event is shown in Fig. 12c. The anomaly maximum associated with the MSR is localized at 65° E. We also find a rather large anomaly at about 30° W. As shown in the next chapter, the winter MSR events are in general dominated by larger amplitudes on wavenumbers 2 or 3, rather than on wavenumber 4. In the spring (and summer) we usually find that wavenumber 4 has a larger amplitude than wavenumbers 2 and 3. For the event shown in Fig. 12c, the amplitudes for the wavenumbers 1 to 4 were 147 m, 71 m, 66 m and 117 m, respectively.

During the summer season the MSR events are rather rare. The event shown in Fig. 4c has its MSR at about 10° E. As in the spring, wave number 4 is seen to be important. The anomaly pattern for this case is shown in Fig. 12d, showing three rather strong anomalies close to 60° N.

A typical MSR event during the fall season is shown in Fig. 4d. The anomaly pattern for this event is given in Fig. 12e. It is seen to have only one area with large amplitude close to the normal position of the ridge in October, given in Fig. 3d.

The variety in the anomaly patterns indicates that there may be several physical causes for the formation and maintenance of the MSR (and MST) events. Some may be due to mountain effects as suggested by Charney et al. (1981) and Hoskins & Karoly (1981). Others may be due to heat sources as suggested by Bjerknes (1962) and Hoskins & Karoly (1981). A third cause may be baroclinic effects as advocated by Frederiksen (1982) and Green (1977). It is the intention of the authors to investigate the anomaly patterns associated with the MSR and MST events more thoroughly in a later paper.

6. WAVE DESCRIPTION OF MSR AND MST EVENTS

Even though a MSR or MST event may be considered as a local phenomenon, the circulation in large areas is affected. Therefore, an analysis of the amplitudes and phases for the Fourier field will be a useful tool for classifying the events. Also the relation between these events and the stationary forcings in middle latitudes like mountains and heat sources will be elucidated from a wave analysis.

A description of the climatology of zonal wavenumbers 1–6 has earlier been given by e.g. Reiter & Westhoff (1981). However, we will here briefly point out some of the characteristics of the first four wavenumbers as they appear from our data. In Figs. 13 and

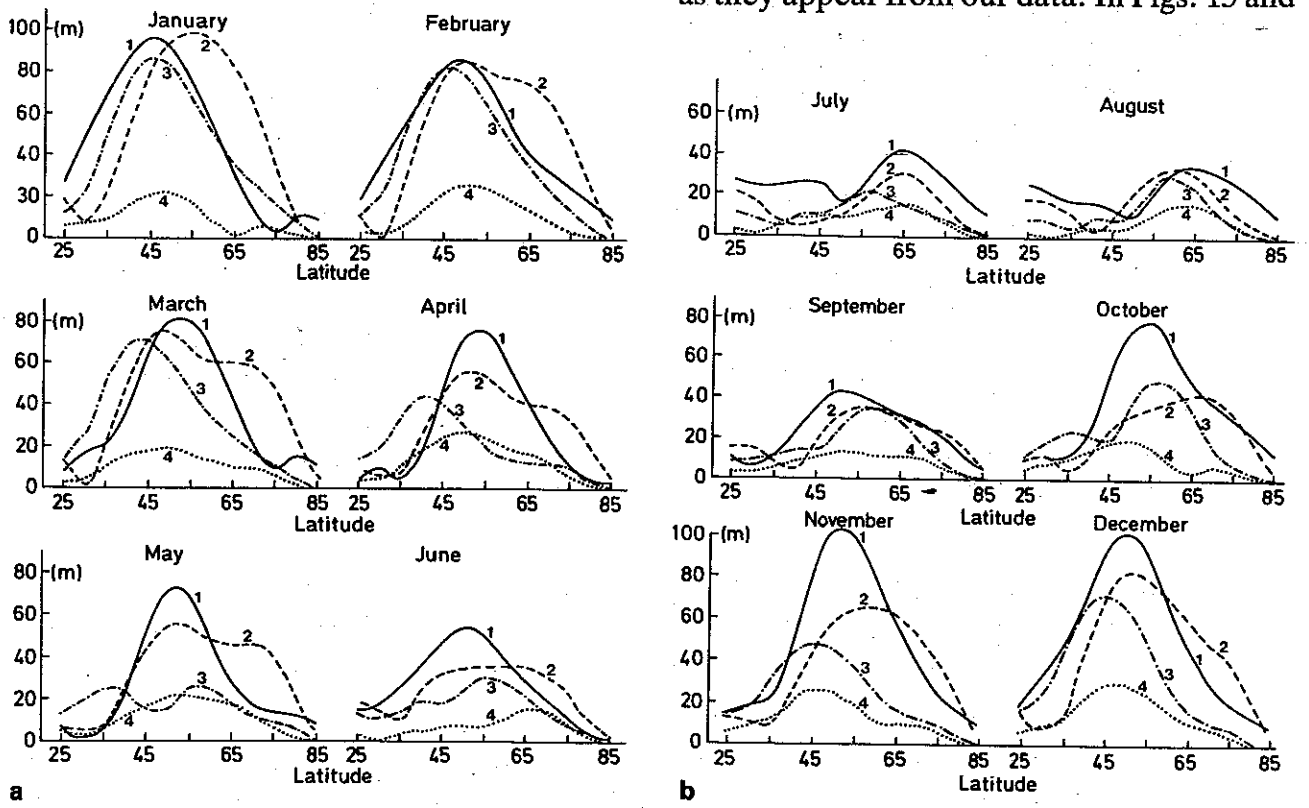

Fig. 13. Amplitudes for wavenumbers 1–4 for the monthly mean fields as functions of the latitude.

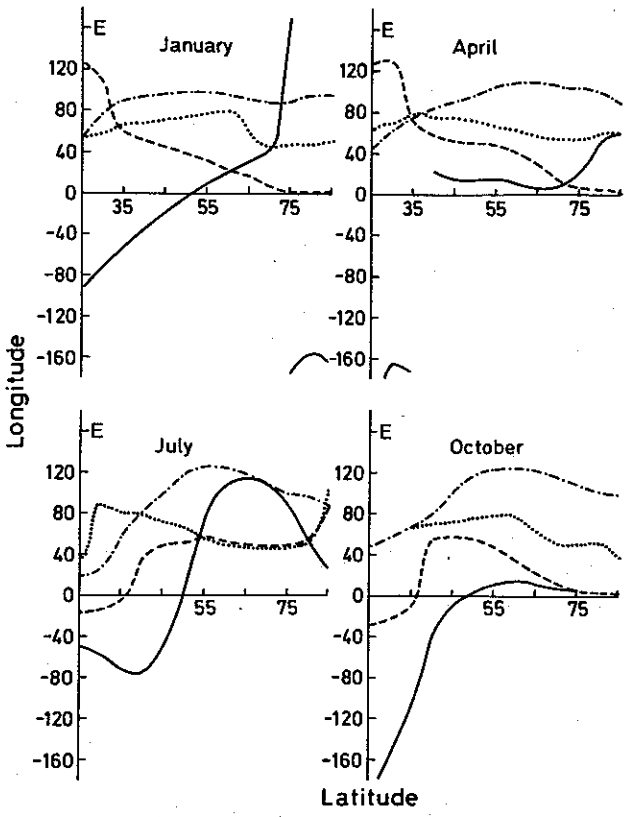

Fig. 14. Phases for wavenumbers 1–4 for the monthly mean fields as functions of the latitude.

14 the amplitudes and phases, respectively, for first four wavenumbers for the monthly mean fields are given as functions of latitude.

As seen from these figures, the amplitudes remain small from June to September. In autumn the longest waves start growing first, and they decay latest in springtime. We find also a rapid shift in the phase at latitudes where the amplitude is small. The further discussion will be based on meridionally averaged fields.

In Fig. 15 the monthly climatic mean z*-field for January is meridionally averaged over the latitude band 40° N–60° N and decomposed onto wavenumbers 1–4. In Fig. 16 the April values are given. January is typical for the winter period November–March. We find the strongest ridge slightly west of Greenwich and the deepest trough in the Pacific near 150° E. This is consistent with Tables 9 and 10, showing that the MSR and MST events in wintertime are mostly found in these two regions, respectively.

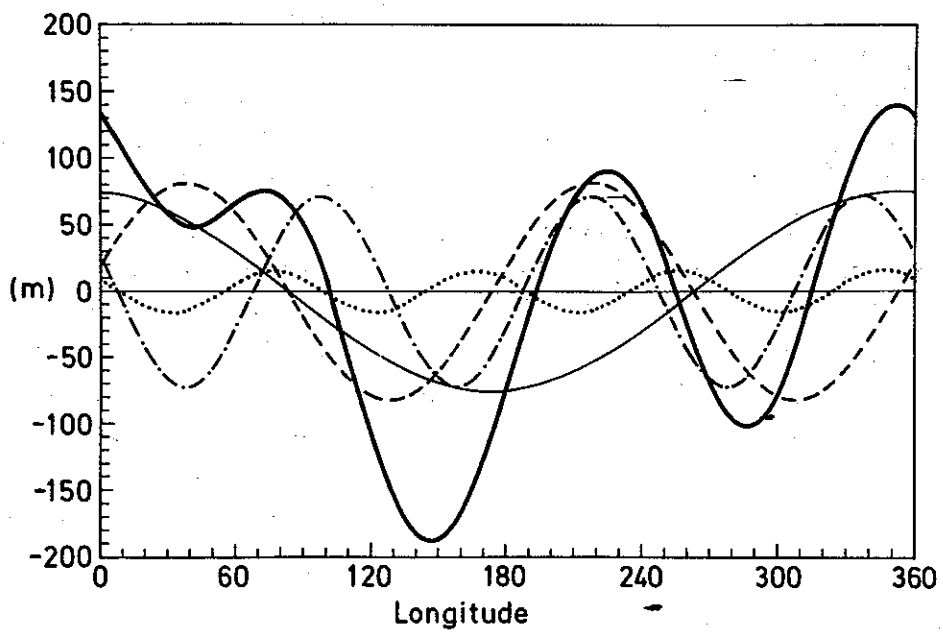

Fig. 15. The mean January amplitudes for wavenumber 1–4 and the total amplitude as a function of the longitude. Thick solid curve, the total amplitude. Thin solid curve, wavenumber 1. Dashed curve wavenumber 2. Dash-dotted curve wavenumber 3. Dotted curve wavenumber 4.

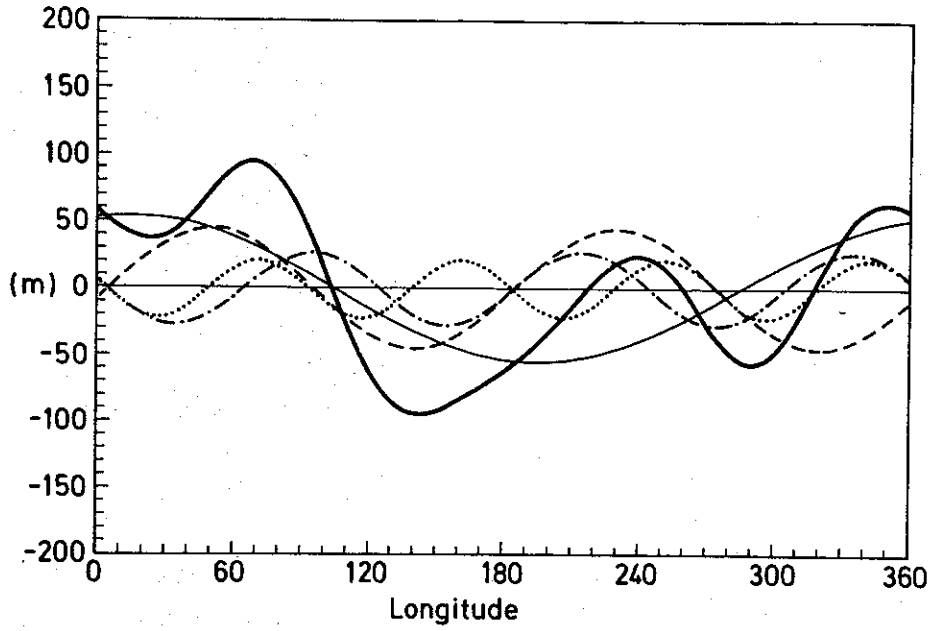

Fig. 16. As Fig. 15, but for April.

In April the picture is changed. The ridge at 70° E grows up and is now the strongest. The MSR events are also most frequent near 60° E in April and May. The deepest trough is located about 150° E, and most of the MST events in this period are found in the region 140–190° E.

The winter MSR events in the Atlantic–European region will be investigated in some detail. For this purpose the three sectors 30–20° W, 5° W–5° E and 20–30° E are selected. For each sector we have computed the amplitude, the amplitude ratio relative to January climatic mean and the phase deviation from January climatic mean for wavenumbers 1–4. The relative amplitude and phase shift averaged over all events in each sector are found to be:

Sector 20°–30° W: 1.86, 10° W; 0, 85, 10° W; 1.84, 7° W and 4.46, 7° W
Sector 5° W–5° E: 1.38, 14° E; 1.65, 12° W; 2.07, 10° E and 2.28, 18° E
Sector 20°–30° E: 2.56, 36° E; 1.80, 0°; 1.82, 32° E and 8.64, 27° E

The high value (8.64) of the relative amplitude for wavenumber 4 is due to two exceptionally high values. However, these values are of minor importance since the normal amplitudes are small for these cases. Excluding these two numbers, the average relative amplitude used in Figs. 17–19 is reduced to 4.1.

The relative importance of each wavenumber is different for each sector. The sector 20–30 E is close to a climatological ridge for wavenumber 2, and here wavenumber 2 has a larger amplitude than wavenumber 3. The mean amplitudes for these waves are 161 and 67 m, respectively. However, for the sector 30–20° W, where wavenumber 3 has a climatological ridge (Fig. 15), this wavenumber has a larger amplitude than wavenumber 2 for 12 of 14 events in this sector. The mean amplitudes for the 14 events are 114 and 72 m, for the wavenumbers 3 and 2 respectively. This result differs from what was found by Austin (1980).

For all three sectors the increase in the partial amplitudes is of importance.

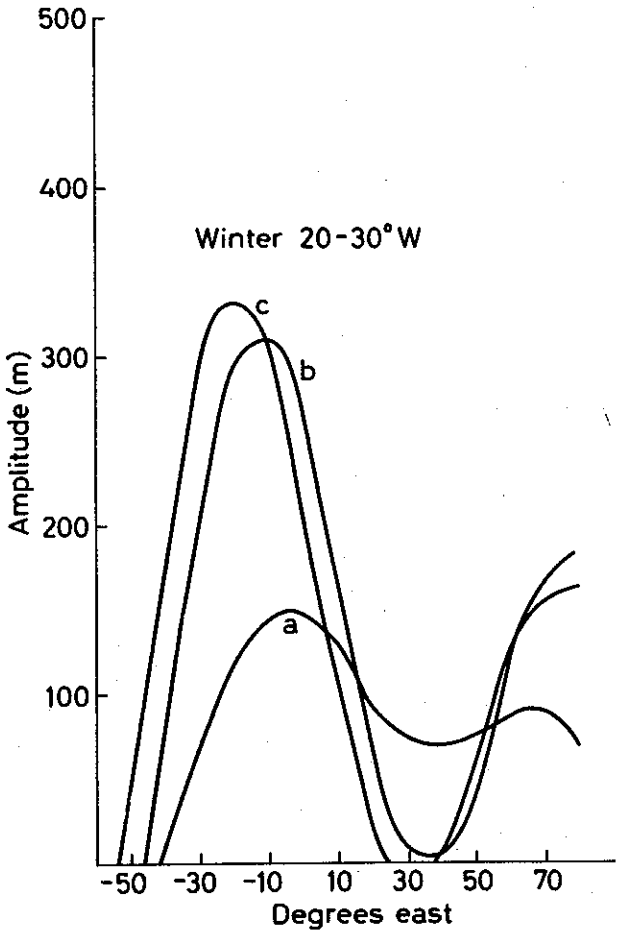

Fig. 17. Mean amplitude for the MSR events in the 20–30° W sector for the winter months. a) The height deviation for a mean January month. b) The height deviation if the four amplitudes are multiplied by the relative amplitudes given in the text. c) The height deviation if also the phase shift is taken into account.

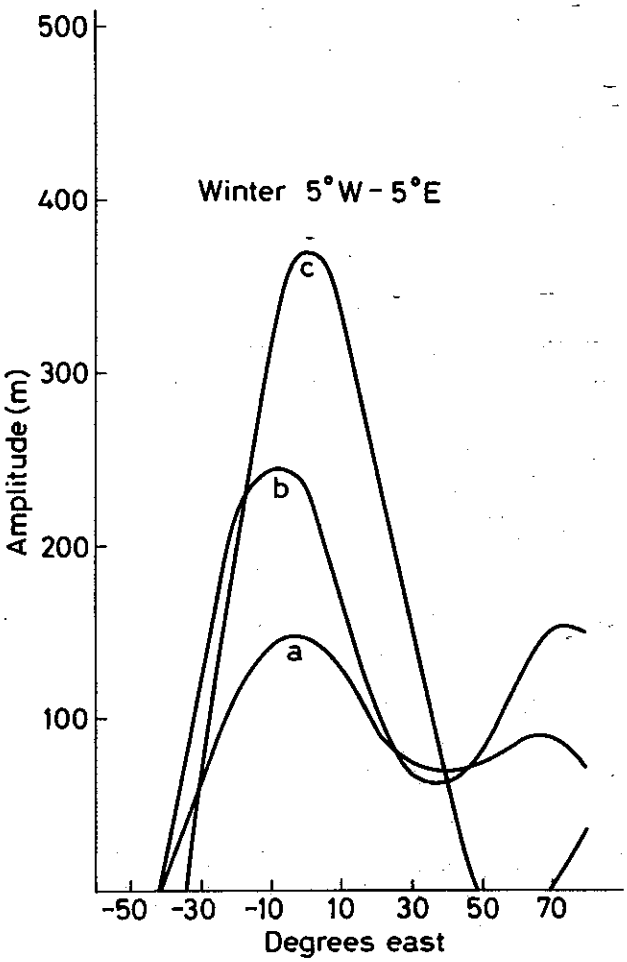

Fig. 18. The same as Fig. 17 for the 5° W–5° E sector.

However, the phase shift acts differently in the three sectors, as seen from the figures. The effect is mainly a shift in position for the 20–30° W sector. In the Greenwich sector it causes an increased amplitude, and for the 20–30° sector it influences both the amplitude and position.

As seen from Fig. 16, the field has a secondary minimum at about 20° E. Therefore the probability of finding MSR events in this sector is reduced. However, as seen from Table 9, 6 MSR events are found in the sector 20–30° E. Therefore, the relative amplitude and phase shift are calculated for two sectors: Sector 20–30° E; 2.90, 20° E; 2.42, 2° E; 3.04, 29° E and 2.78, 22° E.

Sector 50–70° E; 1.63, 14° E; 1.74, 12° E; 1.82, 30° W and 3.14, 7° W.

The resulting amplitudes are shown in Figs. 20 and 21. As seen, both the increased amplitudes and phase shift are of importance.

In the Pacific region a large amplitude on wavenumber 1 will reduce the chances of MSR-events if it is in normal position. Nevertheless, 8 of 16 winter MSR-events are found in the Pacific when wavenumber 1 is greater than normal. In one case (January 1947) the amplitude ratio is as large as 6.5. In these

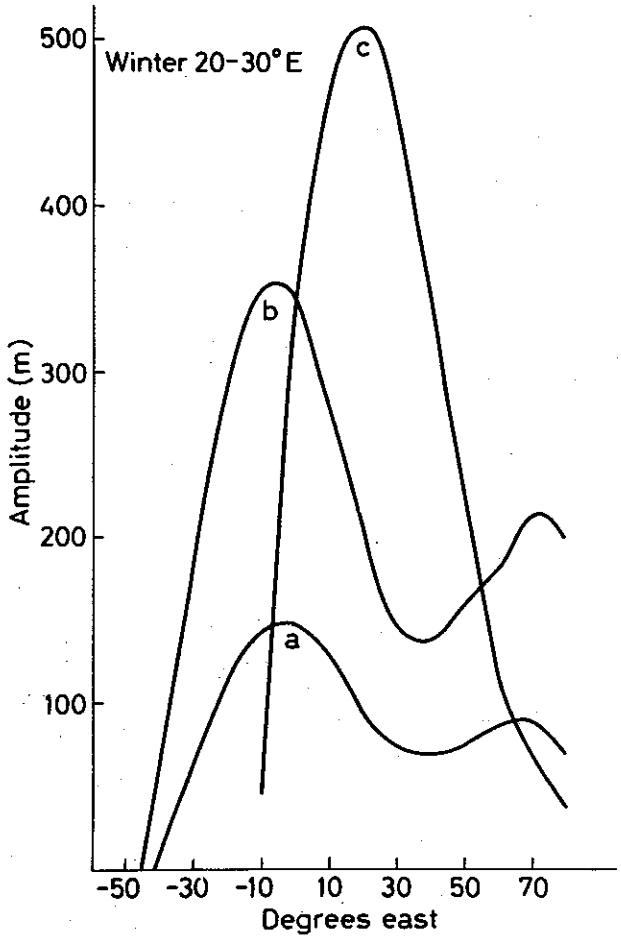

Fig. 19. The same as Fig. 17 for the 20–30° E sector.

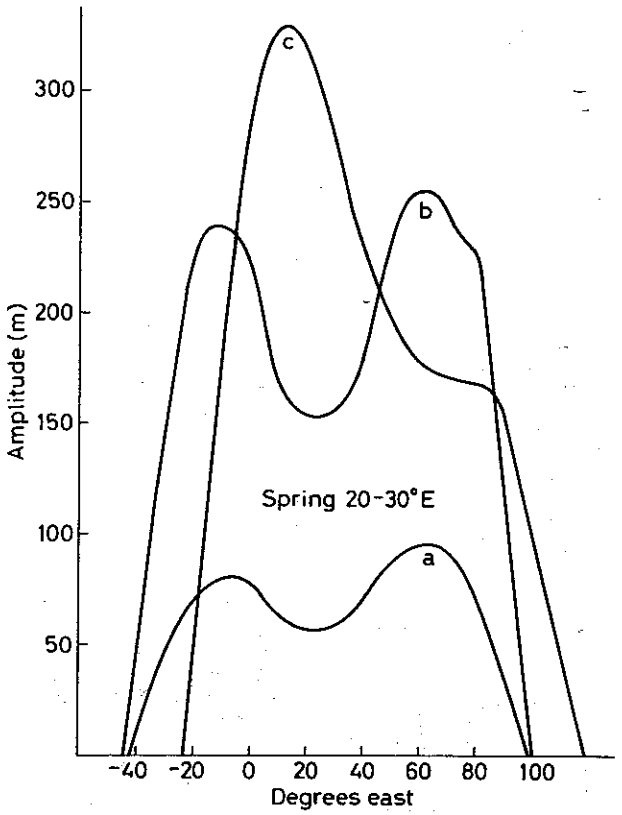

Fig. 20. The same as Fig. 17 for the 20–30° E sector at spring time.

cases, however, the phase of wavenumber 1 is shifted up to 150° in either direction. Also this result differs from that of Austin (1980).

It may be of some interest to compare the phases of wavenumbers 1–4 with the phases of the topography. The topographical data given by Berkofsky Bertoni (1955) are Fourier analyzed and the Fourier components are given in Table 11 for wavenumbers 1–4.

In Table 12 the phase differences between the zonal waves in the 500 mb heights and the corresponding 'waves' in the topography are calculated in units of half wavelengths. For wavenumber 1 a value of +0.5 means that the ridge in the 500 mb wave is 90° east of the corresponding ridge of the topography.

For simplicity, we have averaged the topography meridionally from 25° N to 60° N, and compared the phase of the topography and the 500 mb height fields in Figs. 15 and 16. For the four wavenumbers the first ridge of the topography is localized near 85° E, 80° E, 105° E and 0° E, respectively. From this comparison we find that for wavenumbers 1 and 2, the 500 mb ridge is a quarter of a wavelength upstream of the topographical ridge, whereas wavenumbers 3 and 4 are in phase with the topography. This indicates that the waves behave as in a barotropic fluid and that the critical wavenumber K (Held 1983) lies between 2 and 3.

7. CONCLUDING REMARKS

In this paper the 500 mb data for the period 1946–1980 are analysed in order to identify major quasistationary ridges and troughs. In all, 510 such events are found, and they

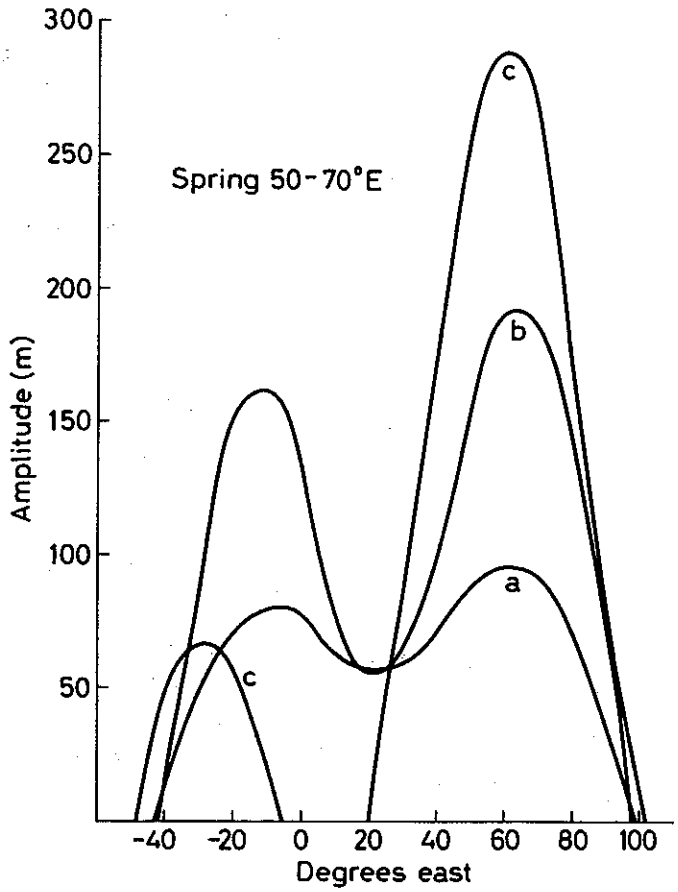

Fig. 21. The same as Fig. 17 for the 50–70° E sector at spring time.

are most frequent in wintertime, November through March. The duration of the events may be estimated from first order Markov chain.

As expected, there are two preferred regions for the stationary troughs, the Atlantic and Pacific regions. The ridges, however, may be divided into three groups, located at the Pacific, the Atlantic-European and the Asian region. While 82% of the troughs are found in the Pacific region, only 10% of the ridges are localized in that region. Most of the ridges (67%) are found in the Atlantic-European region.

Several papers concerning blocking phenomena in wintertime have been published. In spite of using different criteria, most of the winter blocking events published

Table 11
The amplitudes A and phases B obtained by Fourier expansion of the topography.

A, B	Latitude										
	65	60	55	50	45	40	35	30	25		
A_0	750	626	555	733	876	1182	1521	1170	594		
A_1	164	249	167	222	269	476	1026	866	316		
B_1	−169	−170	142	104	78	71	80	79	66		
A_2	147	112	216	384	391	661	1089	781	222		
B_2	−26	39	−86	90	84	76	81	84	80		
A_3	75	214	223	274	355	193	592	552	204		
B_3	−18	−3	0	−4	−2	−6	−32	−28	−4		
A_4	272	210	71	167	310	252	692	586	233		
B_4	45	44	34	5	3	−6	−7	−2	8		

Table 12

Phase shift between the $Z^*(\varphi)$ field and the topography. Unit; half the wavelength. Positive sign indicates that the $Z^*(\varphi)$ field is shifted eastward relative to the topography.

	Latitude								
Wave no.	65	60	55	50	45	40	35	30	25
					January				
1	−.89	−.94	−.74	−.59	−.53	−.59	−.76	.84	.90
2	.49	−.69	−.68	−.56	−.43	−.27	−.23	.27	.59
3	−.15	−.35	−.35	−.28	−.37	−.37	−.02	−.25	.95
4	.33	.84	.98	−.44	−.44	−.36	−.40	−.71	−.96
					February				
1	−.89	−.97	−.77	−.62	−.53	−.56	−.73	−.83	−.85
2	.46	−.16	−.64	−.52	−.46	−.27	−.30	−.17	.58
3	−.05	−.25	−.30	−.28	−.32	−.37	−.02	−.25	1.00
4	.40	.51	.78	−.58	−.44	−.29	−.33	.78	.98
					March				
1	−.97	−.99	−.74	−.54	−.45	−.48	−.80	−.94	−.93
2	.48	−.09	−.61	−.52	−.43	−.30	−.37	.68	.52
3	.05	−.20	−.30	−.28	−.37	−.42	−.08	−.30	.45
4	.49	.64	.91	−.29	−.18	.04	.13	−.04	−.56
					April				
1	.98	−.99	−.71	−.49	−.35	−.28	.59	.64	.48
2	.62	.04	−.51	−.42	−.36	−.20	−.13	.51	.52
3	.10	−.15	−.25	−.33	−.47	−.52	−.23	−.50	.80
4	.29	.44	.71	−.49	−.38	−.22	−.13	−.44	−.76
					May				
1	−.91	−.97	−.67	−.46	−.35	−.36	−.66	−.84	−.20
2	.56	.04	−.44	−.31	−.20	−.07	−.13	.91	.89
3	.35	.15	.15	.07	−.42	−.62	−.33	−.60	.75
4	.22	.31	.64	−.62	−.44	−.22	−.13	−.51	−.89
					June				
1	−.44	−.61	−.52	−.44	−.45	−.58	−.74	−.76	−.58

2	.62	.08	−.38	−.22	−.13	−.07	−.40	−.89	−.98
3	.35	.15	.10	.07	−.27	−.47	−.13	−.80	.55
4	.09	.18	.58	−.56	−.44	−.09	.00	−.98	.78
					July				
1	−.42	−.47	−.39	−.57	−.73	−.81	−.84	−.76	−.63
2	.82	.14	−.38	−.42	−.40	−.47	−.97	.90	.91
3	.25	.10	.05	.02	−.37	−.62	−.53	.85	.35
4	.00	.11	.44	−.64	−.44	−.16	−.07	−.02	.64
					August				
1	−.49	−.51	−.36	−.51	−.75	−.83	−.83	−.73	−.63
2	.72	.04	−.51	−.46	−.40	.90	.83	.83	.94
3	.40	.15	.10	.02	−.47	−.67	−.63	.85	.40
4	.00	.04	.18	−.91	−.58	−.22	−.20	.89	.64
					September				
1	−.54	−.67	−.59	−.56	−.55	−.68	−.88	−.76	−.53
2	.62	.01	−.51	−.42	−.33	−.17	.77	.81	.89
3	.30	.10	.00	−.03	−.37	−.67	−.48	−.85	.50
4	.22	.31	.64	−.62	−.58	−.36	−.40	−.84	.64
					October				
1	−.99	−.97	−.72	−.56	−.48	−.61	.92	.69	.55
2	.56	−.02	−.51	−.39	−.30	−.23	.97	.81	.79
3	.35	.10	.05	.02	−.27	−.62	−.38	−.60	.85
4	.42	.78	.98	−.42	−.44	−.36	−.40	−.71	.98
					November				
1	.91	.93	−.79	−.59	−.50	−.54	−.86	.81	.65
2	.59	−.02	−.69	−.48	−.43	−.37	−.70	.80	.64
3	−.05	−.30	−.35	−.33	−.47	−.52	−.18	−.55	.80
4	.20	.38	.64	−.71	−.64	−.56	−.53	−.71	−.89
					December				
1	−.97	.99	−.77	−.61	−.43	−.59	−.81	−.99	.87
2	.56	−.06	−.64	−.56	−.47	−.33	−.40	.60	.54
3	−.15	−.32	−.40	−.33	−.42	−.42	−.08	−.35	−.70
4	.53	.64	.84	−.51	−.51	−.42	−.47	−.78	−.96

by Charney et al. (1981) and Dole (1978) may be identified as major ridges in this paper.

A comparison with the early published survey of blocking events by Rex (1950) reveals some deviation. The conformity is best for blocking events in the Atlantic region in wintertime. The discrepancy may be due to different definitions and data. This assumption seems plausible since many of Rex's physical reasonings are in agreement with our results.

The anomaly patterns found show a large variety. However, some patterns are found to be typical for each season. The anomaly patterns and the wave description indicate clearly that wavenumber 4 is relatively most important in the spring and summer. The wave description indicates also that the events are associated with an amplification of the wave amplitudes near the normal position. In addition the analyses show that a relatively small phase shift for the shorter waves may intensify the ridge or trough and shift the position of the anomaly patterns away from the normal position. Wavenumbers 1 and 3 have a trough in the Pacific and European region, respectively. Consequently no ridges in these regions are expected if the amplitudes of the mentioned waves are large. Nevertheless, stationary ridges are found in these regions, illustrating the effect of the phase shift, as pointed out in section 6.

ACKNOWLEDGEMENTS

This work has been supported by the Norwegian Research Council for Science and the Humanities (NAVF) under contract no. D10.09-027 'Atmospheric Circulation Types and Climate'. The authors wish to thank Prof. A. Eliassen and Prof. R. Fjørtoft for valuable discussions.

REFERENCES

Austin, J. F. 1980. *Quart. J.R. Met. Soc. 106*, 327.

Berskofsky, L. & Bertoni, E. A. 1955. *Bull. Am. Met. Soc. 36*, 350.

Bjerknes, J. 1962. *Geofysiske Publikasjoner 24*, 115.

Charney, J. A., Shukla, J. & Mo, K. C. 1981. *J. Atmos. Sci. 38*, 762

Dole, R. M. 1978. Private communication.

Dole, R. M. 1983. p. 95 in *Large-Scale Dynamical Processes in the Atmosphere.* Academic Press.

Frederiksen, J. S. 1982. *J. Atmos. Sci. 39*, 969.

Garriot, E. B. 1904. Long range forecasts. *U.S. Wea. Bur. Bull. 35.*

Green, J. S. A. 1977. *Weather 32*, 120.

Held, I. M. 1983. p. 127 in *Large-Scale Dynamical Processes in the Atmosphere.* Academic Press.

Hoskins, B. J. & Karoly, D. 1981. *J. Atmos. Sci. 38*, 1179.

Jenne, R. L. 1975. Data sets for meteorological research. NCAR Tech. Note TN/IA-111. NCAR, P.O. Box 3000, Boulder, Co. 80307, U.S.A.

Labitzke, K. 1977. *Mon. Wea. Rev. 105*, 762.

Lejenäs, H. & Økland, H. 1983. *Tellus 35A*, 350.

Namias, J. 1964. *Tellus 16*, 394

Reiter, E.R. & Westhoff, D. 1981. *J. Atmos. Sci. 38*, 732

Rex, D. P. 1950. *Tellus 2*, 196 and 275.

Wallace, J. M. & Gutzler, D. S. 1981. *Mon. Wea. Rev. 109*, 784.

A unified theory of interhemispheric electron transport and energy degradation

KNUT STAMNES
The Auroral Observatory, Institute of Mathematical and Physical Sciences, University of Tromsø

Stamnes, K. A unified theory of interhemispheric electron transport and energy degradation. *Geophysica Norvegica*, Vol. 33, No. 1, pp. 41–51, 1985.

A unified theory of interhemispheric electron transport and thermalization based on the electron transport equation derivable for the electron continuity equation is provided. Except for wave-particle interactions, this equation adequately describes all other relevant plasma and neutral gas collision processes occurring in the entire geomagnetic field tube connecting conjugate hemispheres. This approach avoids the tedious book-keeping procedures used in previous approaches that combined a Fokker-Planck approach in the plasmasphere with a transport equation formulation in both hemispheres. Detailed solutions to the electron transport equations are presented in the two-stream approximation. The theory can be used to compute production rates of various excited states and to predict ambient electron gas heating for solar EUV produced photoelectrons as well as for auroral electrons.

K. Stamnes, The Auroral Observatory, Institute of Mathematical and Physical Sciences, University of Tromsø, P.O. Box 953, *N*-9001 *Tromsø, Norway.*

1. INTRODUCTION

Problems involving electron impact excitation of aurora, airglow and electron heating of planetary ionospheres require solutions of the equation describing transport and thermalization of energetic electrons constrained to move along magnetic field lines in the ionosphere-magnetosphere. For applications to the ionosphere it has been customary to utilize some form of a transport equation derivable from the Boltzmann equation to describe the electron behaviour (e.g. Nisbet 1968, Banks & Nagy 1970, Nagy & Banks 1970, Stolarski 1972, Mantas 1975, Swartz 1972, 1976, Strickland et al. 1976, Oran & Strickland 1978, Swartz & Stamnes 1977, Stamnes 1977, 1980, 1981a, b). All these papers and many others dealt with ionospheric effects of electron energy deposition in only one hemisphere, ignoring the coupling with the plasmasphere and the conjugate ionosphere. The first attempt at a comprehensive description of energetic electron interaction with the plasma inside a magnetic field tube connecting conjugate hemispheres, is due to Lejeune & Wormser (1976). Rather than using a transport formulation, Lejeune & Wormser used a Fokker-Planck approach to describe the collisional interactions between the energetic electrons and the ambient magnetospheric plasma, and no attempts were made to take into account the adjacent ionospheres. Mantas et al. (1978) combined solutions to the electron transport equation (Mantas 1975) in both ionospheres with the results of Lejeune & Wormser for the plasmasphere to obtain a solution for the

entire field tube. This solution was arrived at in an iterative fashion in which results for the separate regions were matched at the boundaries. A somewhat similar procedure had previously been utilized by Swartz et al. (1975) and was subsequently employed by Lejeune (1979b). Although there is nothing wrong in principle with such a hybrid approach, it does involve tedious book-keeping procedures which would be avoided by a formulation that treats the entire field tube as a single unit.

The primary purpose of the present paper is to provide a unified theoretical description of interhemispheric electron transport and thermalization. It will be shown that the electron transport equation provides an adequate description of all the relevant plasma and neutral gas collision processes (except for wave-particle interactions) occurring inside a field tube connecting conjugate hemispheres. Thus, there is no need to use a different formulation in the plasmasphere than in the ionosphere. A unified treatment is not only conceptually appealing; it also considerably simplifies the practical numerical implementation of the solutions. Detailed solutions to the electron transport equation, including the magnetic mirroring term, are provided in the two-stream approximation.

A secondary purpose of this paper is to review and compare the transport and Fokker-Planck equations and discuss their validity with respect to the particular problem at hand: namely, energetic electron energy deposition and transport in a partially ionized gas. From this discussion we conclude that while the transport equation provides a suitable description of electron interaction in a neutral or weakly ionized gas, as well as a fully ionized plasma (which makes a unified treatment possible), the Fokker-Planck aproach does not provide an adequate description of electron transport and thermalization in a neutral (or weakly ionized) gas for two reasons: Both the small-angle scattering assumption and the continuous slowing down approximation (under-lying the Fokker-Planck approach) break down at low electron energies (below about 1 keV and 100 eV respectively).

2. TRANSPORT AND FOKKER-PLANCK EQUATIONS

The interaction of suprathermal electrons with the partially ionized gas in the ionosphere–plasmasphere is described by the electron continuity equation

$$\frac{\partial f(\mathbf{r}, \mathbf{v}, t)}{\partial t} + \mathbf{v} \cdot \nabla_r(\mathbf{r}, \mathbf{v}, t) + \nabla_v[\dot{\mathbf{v}} f(\mathbf{r}, \mathbf{v}, t)] = Q(\mathbf{r}, \mathbf{v}, t) \quad (1)$$

where f (in units $cm^{-6}\,s^3$) is the distribution function, $\mathbf{r}$ is the position vector, $\mathbf{v}$ the velocity vector, and Q (in units $cm^{-6}\,s^2$) a source (sink) term due to scattering and production of electrons (e.g., due to solar EUV radiation). For conservative systems (for which $\nabla_v \dot{\mathbf{v}} = 0$) eq. (1) reduces to the Boltzmann equation

$$\frac{\partial f(\mathbf{r}, \mathbf{v}, t)}{\partial t} + \mathbf{v} \cdot \nabla_r f(\mathbf{r}, \mathbf{v}, t) + \dot{\mathbf{v}} \cdot \nabla_v f(\mathbf{r}, \mathbf{v}, t) = Q(\mathbf{r}, \mathbf{v}, t) \quad (2)$$

which, when no sources or sinks are present, is commonly referred to as Liouville's theorem or the Vlasov equation.

Transport equation

Starting with eq. (1), one can derive a transport equation describing the steady-state behaviour of suprathermal electrons in a flux tube in the ionosphere–magnetosphere

(Stamnes 1980, Stamnes & Rees 1983)

$$\frac{dI(z, E, \alpha)}{dy} - n_e(z)\frac{\partial}{\partial E}[L(E)I(z, E, \alpha)]$$

$$= -\sum_j n_j \sigma_j^{tot}(E) I(z, E, \alpha)$$

$$+ \sum_j n_j(z)\sigma_j^{el}(E)$$

$$\times \tfrac{1}{2}\int_0^{\pi} p_j^{el}(\alpha, \alpha')I(E, z, \alpha')\sin\alpha' \, d\alpha'$$

$$+ \int_{E'>E}^{\infty} dE' \sum_j n_j(z)\sigma_j^{in}(E, E')$$

$$\times \tfrac{1}{2}\int_0^{\pi} p_j^{in}(\alpha, \alpha')I(z, E', \alpha')\sin\alpha' \, d\alpha'$$

$$+ P(z, E, \alpha). \qquad (3)$$

The first term on the left side is the change in the intensity (in units $cm^{-2}\,s^{-1}\,ster^{-1}\,eV^{-1}$) per unit path length, dy, along the electron trajectory. z denotes altitude, E energy, and α pitch angle. The second term on the left side stems from the third term on the left side of eq. (1). It describes the continuous slowing down of the suprathermal electrons due to collisions with the ambient electron gas. It is arrived at by assuming that there is a frictional force acting on the fast electrons defined by

$$m\dot{v} = -n_e L(E)\frac{\mathbf{v}}{v} \qquad (4)$$

where n_e is the electron density, and L(E) the stopping cross section (cf. Stamnes & Rees 1983 for a detailed derivation). The terms on the right side of eq. (3) are the changes in the electron intensity caused by 1) scattering out of the beam (to other directions and energies), 2) elastic scattering into the beam, 3) cascading from higher energies including production of secondaries, tertiaries etc., and 4) production of primary electrons. $n_j(z)$ is the density and $\sigma_j^{tot}(E)$ the sum of the total elastic, $\sigma_j^{el}(E)$, and inelastic, $\sigma_j^{in}(E)$, cross sections of species j. $p_j(\alpha, \alpha')$ is the azimuthally-averaged angular cross-section or phase function which is normalized so that $\frac{1}{2}p(\alpha, \alpha')$ gives the probability of scattering from pitch angle α' into α.

While the summation in the first and second terms on the right side of eq. (3) extends over neutral species and ions (for ions $\sigma_j^{tot} = \sigma_c$ the (elastic) Coulomb cross section), only neutral species are included in the third term on the right side of eq. (3). This treatment is consistent with the continuous slowing down approximation (eq. (4)) which is based on the premise that Coulomb collisions with the ambient electrons lead to energy loss (described by the second term on the left side) but no deflections, whereas Coulomb collisions with the much heavier ions lead to angular scattering only.

Conservation of the first adiabatic invariant (i.e. magnetic moment) implies (Lejeune & Wormser 1976, Prather et al. 1978)

$$\frac{dI}{dy} = \mu\frac{\partial I}{\partial s} - \frac{(1-\mu^2)}{2}\frac{1}{B}\frac{\partial B}{\partial s}\frac{\partial I}{\partial \mu} \qquad (5)$$

where $ds = dz/\sin\theta_D$ denotes path length along the magnetic field line, $\mu = \cos\alpha$, θ_D is the geomagnetic dip angle at altitude z, and B is the geomagnetic field strength. Thus, eq. (3) may be rewritten as

$$\mu\frac{\partial I(z, E, \mu)}{\partial s} - \frac{(1-\mu^2)}{2}\frac{1}{B}\frac{dB}{ds}\frac{\partial I(z, E, \mu)}{\partial \mu}$$

$$- n_e(z)\frac{\partial}{\partial E}[L(E)I(z, E, \mu)]$$

$$= -\sum_j n_j(z)\sigma_j^{tot}(E)I(z, E, \mu)$$

$$+ \sum_j n_j \sigma_j^{el}(E)$$

$$\times \tfrac{1}{2}\int_{-1}^{1} p_j^{el}(\mu, \mu')I(z, E, \mu')\, d\mu'$$

$$+ \int_{E'>E}^{\infty} dE' \sum_j n_j(z)\sigma_j^{in}(E, E')$$

$$\times \tfrac{1}{2}\int_{-1}^{1} p_j^{in}(\mu, \mu')I(z, E', \mu')\, d\mu'$$

$$+ P(z, E, \mu). \qquad (6a)$$

Equation (6a) is valid under the following assumptions: 1) the gyroperiod is much less than the average collision time so that azimuthal symmetry prevails, 2) particle acceleration caused by external electric fields is neglected, and 3) no collective or non-linear effects are included. Prather et al. (1978) derived a transport equation similar to eq. (6a), but considered only isotropic elastic scattering. In Section 4 we show how to include anisotropic elastic scattering by neutrals as well as ions. For applications to realistic situations this extension is essential.

To facilitate a comparison with the Fokker-Planck equation given below, we note that for a fully ionized proton/electron gas embedded in a constant, vertical magnetic field (i.e. $\sin\theta_D = 1$), eq. (6a) reduces to

$$\mu\frac{dI(z, E, \mu)}{dz} = n_e(z)\left\{\frac{\partial}{\partial E}[L(E)I(z, E, \mu)]\right.$$

$$+ \frac{\sigma_c(E)}{2}\int_{-1}^{1}[p_c(\mu, \mu')$$

$$\left. - 2\delta(\mu - \mu')]I(z, E, \mu')d\mu'\right\} \qquad (6b)$$

where $\delta(\mu - \mu')$ is the Dirac delta-function, $\sigma_c(E)$ is the screened Coulomb cross section and p_c the corresponding phase function (expressions for σ_c and p_c are given in Sect. 4). The first term on the right side of (6b) describes 'slowing-down' due to collisions with ambient electrons and the second term elastic scattering in angle. Equation (6b) applies also to electron penetration in a neutral gas if $n_e(z)$ is replaced by the neutral gas density, L(E) is interpreted as the neutral gas stopping cross section including losses due to excitations and ionizations, and $\sigma_c(E)$ and $p_c(\mu, \mu')$ are replaced by the appropriate elastic cross section and phase function describing electron interaction with the neutral gas under consideration. Note, however, that for electron penetration in a neutral gas eq. (6b) will provide accurate results only for energies above about 100 eV, since the continuous slowing down approximation breaks down at lower energies.

Fokker–Planck Equation

The Fokker-Planck equation for the electron transport and energy degradation problem can be obtained from the Boltzmann equation, eq. (2), (Bethe et al. 1938, Rosenbluth et al. 1957, Montgomery & Tidman 1964, Shkarofsky et al. 1966, Walt et al. 1969) or from the following transport equation derivable from eq. (2), assuming a constant and vertical magnetic field

$$\mu\frac{dI}{dz} = -n(z)\left\{\sigma^{tot}(E)I(z, E, \mu)\right.$$

$$- \int dE'\, \sigma(E, E')$$

$$\left.\times \tfrac{1}{2}\int_{-1}^{1} p(\mu, \mu')I(z, E, \mu')\, d\mu'\right\} \qquad (7)$$

where for simplicity and clarity of exposition summation over species and the primary production term have been omitted.

By expanding the intensity in a Taylor series to first order in E and second order in μ, the following Fokker-Planck equation is obtained (Walt et al. 1969, Strickland &

Bernstein 1976, Strickland et al. 1976)

$$\mu \frac{dI}{dz} = n(z)\left\{\frac{\partial}{\partial E}[L(E)I] + \frac{Q(E)}{2}\frac{\partial}{\partial \mu}\left[(1-\mu^2)\frac{\partial I}{\partial \mu}\right]\right\} \quad (8)$$

where Q(E) is the momentum transfer cross section and L(E) the stopping cross section. The second term on the right side of eq. (8) represents scattering (or diffusion) in angle, while the first term describes energy loss (continuous slowing down approximation).

Comparing eqs. (6b) and (8), one observes that for transport of electrons in a fully ionized or neutral gas the transport equation (in the continuous slowing down approximation) and the Fokker-Planck equation differ only in their treatment of the angular scattering. Thus, it is seen that starting from the continuity equation (1), and invoking the continuous slowing down approximation, eq. (4), one is led to exactly the same slowing down term as is obtained by departing from the Boltzmann equation (2), and using the first-order Fokker-Planck approximation.

Strickland et al. (1976) have compared solutions to the transport equation (6b) and the Fokker-Planck equation [eq. (8)] for electron penetration in a neutral gas (molecular nitrogen). They found that the two equations give very similar results for high electron energies where the elastic scattering cross section is strongly peaked in the forward direction. However, for energies below about 1 keV, eq. (8) becomes inadequate because the small-angle scattering assumption (on which it is based), is no longer valid. This means that while the Fokker-Planck equation provides an adequate description of electron interaction in the plasmasphere where small-angle Coulomb scattering prevails, it will lead to erroneous results if applied to electron transport in the ionosphere. Another limitation of the Fokker-Planck approach is that it treats all losses as continuous processes. This approximation works well if the fractional energy loss per collision is small, but it becomes invalid for applications to the ionosphere, since below about 100 eV an electron can lose an appreciable fraction of its energy in a single collision. Thus it is seen that the Fokker-Planck equation cannot be used as a universal tool to describe the interaction of electrons in the ionosphere–magnetosphere system.

Fortunately, the transport equation (6a) does not suffer from these limitations. It treats inelastic excitation and ionization collisions in a discrete rather than a continuous manner and applies equally well in a fully ionized plasma as in a weakly ionized gas. This observation implies that a unified treatment of electron transport and thermalization based on eq. (6a) is possible that properly describes all relevant collisional interactions (except for wave-particle interactions) with the plasma inside a magnetic field tube connecting conjugate hemispheres. The virtue of this transport equation formulation to the ionosphere/magnetosphere coupling problem is that it includes the essential physical processes but entirely avoids the tedious book-keeping procedures inherent in previous hybrid approaches by Mantas et al. (1978) and Lejeune (1979b) in which a transport equation formulation for the ionospheres is combined with results from a Fokker-Planck formulation for the plasmasphere.

3. METHOD OF SOLUTION

Prior to seeking solutions to eq. (6a), it is convenient to introduce the dimensionless scattering depth, $\tau(E, z)$, to replace the geometric altitude, z, as the independent vari-

and (23b) to yield a second-order differential equation for I^- which is then solved subject to suitable boundary conditions at the top and the bottom of the atmosphere and with appropriate internal sources (e.g. solar EUV produced photoelectrons). The upward intensity is subsequently obtained by solving eq. (23b) for I^+.

For the interhemispheric coupling problem it is awkward to apply boundary conditions in terms of either I^+ or I^-. It is better to rewrite eq. (23) in terms of the flux and mean intensity defined previously, eqs. (25) and (26), as follows:

$$\frac{dF}{d\tau} = X(1-\omega)\bar{I} - 2XfF - X\bar{Q} \tag{31a}$$

$$\frac{d\bar{I}}{d\tau} = X(1-\omega+2\omega\beta)F/\bar{\mu}^2 + fX(C_2 - C_1)\bar{I}/\bar{\mu} - XQ_F/\bar{\mu}^2 \tag{31b}$$

where

$$\bar{Q} = Q^+ + Q^-; \; Q_F = \bar{\mu}(Q^+ - Q^-).$$

Elimination of $\bar{I}$ from (31) leads to a second-order differential equation for the flux, F, which is solved subject to homogeneous boundary conditions at the bottom of the atmosphere in both hemispheres. Physically this zero flux condition implies that there is no net flow of energy through a cross sectional area perpendicular to the flux tube at both ends of the field line. Once a solution to F is determined, the mean intensity is obtained by solving eq. (31a) for $\bar{I}$. The numerical aspects of the solution to equations like (23) or (31) are discussed in detail by Stamnes (1981b) and will not be repeated here.

4. PHASE FUNCTION AND BACKSCATTER RATIO

From an analogy with X-ray interaction with matter, the elastic cross section for scattering of electrons by atoms may be written (Mott 1930) as

$$\sigma_c(\theta) = |f(\theta)|^2 \tag{32}$$

where θ is the scattering angle and the scattering amplitude, $f(\theta)$, is

$$f(\theta) = \frac{8\pi^2 m_e}{h^2} \int_0^\infty \frac{\sin \gamma r}{\gamma r} V(r)\, dr. \tag{33}$$

h is Planck's constant, m_e the electron mass, $\gamma = 4\pi \sin(\theta/2)/\lambda$, and λ is the de Broglie wavelength of the electron. Born's assumption that the incident wave is only slightly disturbed inside the atom, has been invoked to arrive at eq. (33). The well-known divergence of eq. (33) for long-range potentials $V(r) \sim 1/r$ can be avoided by using

$$V(r) = \frac{Ze^2}{r} e^{-r/r_s}, \tag{34}$$

where the exponential factor accounts for the fact that the atomic nucleus is effectively screened by its surrounding electron cloud so that beyond a distance, r_s, the atom appears essentially neutral to an approaching fast electron. For a neutral gas the appropriate screening distance is about one Bohr radius, while for a plasma $r_s \sim \lambda_D$ where λ_D is the Debye length. Using eqs. (34) and (33) one finds

$$f(\theta) = \frac{Ze^2}{pv[1 + 2\varepsilon - \cos\theta]} \tag{35}$$

and consequently

$$\sigma_c(E, \theta) = |f(\theta)|^2 = \frac{Z^2 e^4}{p^2 v^2 (1 + 2\varepsilon - \cos\theta)^2} \tag{36}$$

which is a screened Coulomb or Rutherford cross section. In the limit of no screening (i.e. as $\varepsilon \to 0$ or $r_s \to \infty$) eq. (36) reduces to Rutherford's formula, which can be obtained either from classical mechanics or from quantum mechanics in the Born approximation.

The screening parameter, ε, is given by

$$2\varepsilon = \left(\frac{\lambda}{2\pi r_s}\right)^2 = \frac{1}{S^2} \tag{37}$$

where $S = (2\pi r_s)/\lambda$ is the ratio of the 'circumference' of the atom to the incoming electron wavelength and may be referred to as the 'size parameter' in analogy with light scattering by particulate matter. For electrons in the keV range, this size parameter is large and it increases with increasing energy. As in the case of light scattering by particulate matter, this increase of the size parameter with energy qualitatively explains why for electron scattering by atoms the scattering cross section becomes increasingly peaked in the forward direction with increasing energy.

The total elastic cross section is obtained from eq. (26) as

$$\sigma_c(E) = \int_0^\pi \sigma_c(E, \theta)\, d\cos\theta$$

$$= \left(\frac{Ze^2}{vp}\right)^2 \frac{1}{4\varepsilon(1+\varepsilon)} \tag{38}$$

and the corresponding phase function becomes

$$p_c(\cos\theta) = \sigma_c(E, \theta)/\sigma_c(E)$$

$$= \frac{4\varepsilon(1+\varepsilon)}{[1+2\varepsilon-\cos\theta]^2}. \tag{39}$$

For electron scattering with neutrals, the screening parameter varies smoothly with energy from 10^{-2} at 1 keV to 10^{-4} at 100 keV. For energies below 1 keV, ε may be determined by comparing the probability for scattering more than 90° based on eq. (39) with the more accurate value given by Wedde and Strand (1974) (cf. Stamnes 1981a for details).

In order to use eq. (39) also for Coulomb collisions with ions it is necessary to relate the screening parameter, ε_i, to appropriate plasma parameters. This can be done by requiring

$$\int_0^\pi \frac{d\theta}{(1+2\varepsilon_i-\cos\theta)^2}$$

$$= \int_{\theta_{min}}^\pi \frac{d\theta}{(1-\cos\theta)^2}. \tag{40}$$

where θ_{min} is the minimum scattering angle given by (Longmire 1963, Montgomery & Tidman 1964, Krall & Trivelpiece 1973)

$$\theta_{min} = 2/\Lambda \tag{41}$$

and $\Lambda = 3(kT_e)^{3/2}/e^3(4\pi n_e)^{1/2}$ is the argument of the so-called Coulomb logarithm. T_e is the plasma temperature and n_e its density. Evaluating both sides of eq. (40) we find

$$\int_0^\pi \frac{d\theta}{(1+2\varepsilon_i-\cos\theta)^2}$$

$$= \frac{\pi}{\varepsilon_i(1+\varepsilon_i)} \simeq \pi/\varepsilon_i \tag{42}$$

$$\int_{\theta_{min}}^\pi \frac{d\theta}{(1-\cos\theta)^2}$$

$$= \pi\left\{\frac{2}{\theta_{min}} - 1\right\} \simeq \frac{2\pi}{\theta_{min}}. \tag{43}$$

Thus,

$$\varepsilon_i = \frac{\theta_{min}}{2} = 1/\Lambda \tag{44}$$

may be used to evaluate the screening parameter for electron-plasma interactions.

Finally, the phase function obtained from eq. (39) is (Strickland et al. 1976, Stamnes 1980)

$$p(\mu, \mu') = \frac{1}{2\pi}\int_0^{2\pi} p_c(\cos\theta)\, d\phi$$

$$= \frac{4\varepsilon(1+\varepsilon)(1+2\varepsilon-\mu\mu')}{[(1+2\varepsilon-\mu\mu')^2-(1-\mu'^2)(1-\mu^2)]^{3/2}} \tag{45}$$

and the backscatter ratio becomes simply (Stamnes 1981a)

$$\beta = \frac{1}{2}\int_0^1 d\mu' \int_0^1 d\mu\, p(\mu, -\mu') = [\varepsilon(1+\varepsilon)]^{1/2} - \varepsilon. \quad (46)$$

5. CONCLUSION

A unified theory of interhemispheric electron transport and thermalization is developed. It is shown that all relevant neutral gas and plasma collisional interactions with energetic electrons as well as magnetic mirroring effects taking place in a geomagnetic field tube connecting conjugate hemispheres can be adequately described by an electron transport equation derivable from the electron continuity equation. Suprathermal electron collisions with ambient electrons are assumed to result in energy loss (treated in the continuous slowing down approximation) but no deflections, whereas collisions with the much heavier ions are assumed to lead to scattering in angle only (i.e. no energy loss). The scattering in angle is described by a screened Rutherford cross section and the screening parameter, ε_i, for electron-ion collisions is estimated as $\varepsilon_i = 1/\Lambda$, where Λ is the argument of the so-called Coulomb logarithm.

A detailed solution to the transport equation including the magnetic mirroring term is provided in the two-stream approximation. These two coupled equations are written in terms of the electron flux and mean intensity and must be solved subject to a zero flux (i.e. no net energy flow) condition at the end of the field line in both ionospheres.

REFERENCES

Banks, P. M. & Nagy, A. F. 1970. *J. Geophys. Res. 75*, 1902.

Bethe, H. A., Rose, M. E. & Smith, L. P. 1938. *Proc. Am. Philos. Soc. 78*, 573.

Chandrasekhar, S. 1960. in *Radiative Transfer*, Dover, New York.

Kofman, W. & Lejeune, G. 1980. *Planet. Space Sci. 28*, 661.

Krall, N. A. & Trivelpiece, A. W. 1973. *Principles of Plasma Physics*. McGraw-Hill, New York.

Lejeune, G. 1979a. *J. Geophys. Res. 84*, 1481.

Lejeune, G. 1979b. *Planet. Space Sci. 27*, 561.

Lejeune, G. & Wormser, F. 1976. *J. Geophys. Res. 81*, 2900.

Longmire, C. L. 1963. *Elementary Plasma Physics*. Interscience, New York.

Mantas, G. P. 1975. *Planet. Space Sci. 23*, 337.

Mantas, G. P., Carlson, H. C. & Wickwar, V. B. 1978. *J. Geophys. Res. 83*, 1.

Montgomery, D. C. & Tidman, D. A. 1964. *Plasma Kinetic Theory*. McGraw-Hill, New York.

Mott, N. F. 1940. *Proc. Roy. Soc. A 127*, 658

Nagy, A. F. & Banks P. B. 1970. *J. Geophys. Res. 75*, 6260.

Nisbet, J. S. 1968. *J. Atmos. Terr. Phys. 30*, 1257.

Oran, E. S. & Strickland, D. J. 1978. *Planet. Space Sci. 26*, 1161.

Prather, M. J., McElroy, M. B. & Rodriguez, J. 1978. *Planet. Space Sci. 26*, 131.

Rosenbluth, M. N., MacDonald, W. M. & Judd, D. L. 1957. *Phys. Rev. 107*, 1.

Shkarofsky, I. P., Johnston, T. W. & Bachynski, M. P. 1966. *The Particle Kinetics of Plasmas*. Addison-Wesley, Reading, Mass.

Stamnes, K. 1977. *J. Geophys. Res. 82*, 2391.

Stamnes, K. 1980. *Planet. Space Sci. 28*, 427.

Stamnes, K. 1981a *J. Geophys. Res. 86*, 2405.

Stamnes, K. 1981b. Scientific Report, Geophysical Institute, University of Alaska, UAG R-286.

Stamnes, K. & Rees, M. H. 1983. *J. Geophys. Res. 88*, 6301.

Stolarski, R. S. 1972. *J. Geophys. Res. 77*, 2862.

Strickland, D. J., Book, D. L., Coffey, T. P. & Fedder, J. A. 1976. *J. Geophys. Res. 81*, 2764.

Strickland, D. J. & Bernstein, I. B. 1876. *J. Appl. Phys. 47*, 2184.

Swartz, W. E. 1972. Sci. Rep. 381, Ionos. Res. Lab., Pa. State Univ., University Park.

Swartz, W. E. 1976. *J. Geophys. Res. 81*, 183.

Swartz, W. E. & Stamnes, K. 1977. *J. Geophys. Res. 82*, 2401.

Swartz, W. E., Bailey, G. J. & Moffett, R. J. 1975. *Planet. Space Sci. 23*, 589.

Walt, M. MacDonald, W. M. & Francis, W. E. 1969. p. 534 in *Physics of the Magnetosphere*, edited by R. L. Carovillano. D. Reidel, Hingham, Mass.

Wedde, T. & Strand, T. G. 1974. *J. Phys. Sect. B* 7, 1091.

Instructions to Authors

GEOPHYSICA NORVEGICA

publishes papers in English. When preparing manuscripts for submission, authors should consult current copies of the journal and follow its style as closely as possible.

MANUSCRIPTS

Manuscripts must be typewritten, double spaced throughout, on one side of the paper, with a wide margin. Authors should submit the *original* manuscript (preferably with one copy) to the editor, whose address is shown on page 2 of the cover.

Separate sheets should be used for the following: 1) title page, with the author's name and institution, and, if the title is longer than 40 letters and spaces, a short title not exceeding this limit for use in the running heads; 2) an abstract not exceeding 12 lines (910 letters and spaces) with the name and full postal address underneath of the author to whom communications, proofs, and reprints are to be sent; 3) references; 4) Tables with their headings; 5) legends to Figures.

Brief *Acknowledgements* of grants and other assistance, if any, will be printed at the end of the text.

FIGURES, TABLES AND MATHEMATICAL SYMBOLS

All illustrations are to be considered as Figures. Each graph, drawing, or photograph should be numbered in sequence with arabic numerals, and should be identified on the back by the name of the journal, the author's name, and the Figure number. The top should be indicated. The Figures should be the original drawing. The columns of *Geophysica Norvegica* are 67 mm broad, and the size of the original drawings should be in proportion. Lines must be thick enough to allow for reduction. Letters and numbers should not be less than 2 mm high in the printed illustration. Photographs should be submitted as unmounted glossy enlargements showing good details.

Tables are to be numbered consecutively. Each Table should be typed on a separate sheet, with a descriptive heading that makes the Table self-explanatory.

All Figures and Tables should be referred to in the text by their number. Their approximate position should be indicated in the margin of the manuscript.

All numbered equations and all unnumbered but complicated equations should be typed on separate lines. Equations should be punctuated.

All text material will be set in roman type unless otherwise marked. Hence, all variables and other characters to be set in italic type should be underlined once with a straight line. Vectors and other characters in boldface type should be indicated by underlining with a single wavy line.

No footnotes should be used.

REFERENCES TO LITERATURE

In the text, Brown (1957, p. 9), Brown & White (1961). If more than two authors, Brown et al. (1963). Multiple references: 'As several authors have reported (Brown 1967, Brown & White 1961, Green et al. 1963)', i.e. chronological order, no commas between names and year.

Lists of References are to be unnumbered and in alphabetical order. The international alphabetical order of Scandinavian and German vowels should be observed: Å = AA, Æ and Ä = AE, Ø and Ö = OE, Ü = UE. Indicate 1st, 2nd, 3rd, etc. works by the same author in the same year by a, b, c, etc. (White 1966a). No ditto marks should be used. Titles of journals should be abbreviated according to *World List of Scientific Periodicals*.

Examples:

Cadle, R. D. 1966. p. 83 in *Particles in the Atmosphere and Space*. Reinhold Publishing Corporation, New York.

Craig, R. A. 1965. p. 161 in *The Upper Atmosphere. Meteorology and Physics*. International Geophysics Series, Vol. 8. Academic Press, New York and London.

Eliassen, A. & Kleinschmidt, E. 1957. p. 66 in *Handbuch der Physik*. Vol. 48, Part 2, edited by S. Flügge. Springer-Verlag, Berlin.

Junge, C. 1972. *Quart. J. R. Met. Soc. 98*, 711.

PROOFS

Two copies of the first proof will be sent (page proofs). One copy, duly corrected, should be returned to the editor with the least possible delay. All technical parts of the article, including references, names, figures (numbers, formulae), illustrations, etc. are the responsibility of the authors. Authors will be required to pay for any major alterations they may make.

REPRINTS

Fifty reprints of each article will be supplied free. Additional reprints can be ordered at a charge.